JOC The Journal of Organic Chemistry

Article

pubs.acs.org/joc

Geometry Relaxation-Induced Large Stokes Shift in Red-Emitting Borondipyrromethenes (BODIPY) and Applications in Fluorescent Thiol Probes

Yinghui Chen,[†,‡] Jianzhang Zhao,[†,*] Huimin Guo,[†] and Lijuan Xie[‡]

[†]State Key Laboratory of Fine Chemicals, School of Chemical Engineering, Dalian University of Technology, E-208 West Campus, 2 Ling-Gong Road, Dalian 116024, P. R. China

[‡]Institute of Molecular Medicine, Huaqiao University, 269 Chenghua North Road, Quanzhou 362021, P. R. China

Supporting Information

ABSTRACT: 2-Thienyl and 2,6-bisthienyl BODIPY derivatives (**BS-SS** and **BS-DS**) were prepared that show intense absorption (ε = 65000 M^{-1} cm^{-1} at 507 nm) and a large Stokes shift (96 nm) vs the small Stokes shift of typical BODIPY (<15 nm). Control compounds with a thienyl unit at the 8-position or phenyl substituents at the 2,6-positions were prepared (**BS-1** and **9**). **BS-1** shows absorption/emission in the blue-shifted range and a small Stokes shift (12 nm). Compound **9** shows absorption in the red-shifted range, but the Stokes shift (<30 nm) is much smaller than that for **BS-SS** and **BS-DS**. DFT calculations propose the large Stokes shifts of **BS-SS** and **BS-DS** are due to the remarkable geometry relaxation upon photoexcitation and its substantial effect on the energy levels of molecular orbitals. For the dyes with small Stokes shifts, much smaller geometry relaxations were found. The fluorophores were used for fluorescent thiol probes, with 2,4-dinitrobenzenesulfonyl (DNBS) as the fluorescence switch. Both fluorescence OFF−ON and unprecedented ON−OFF transduction were observed, which are attributed to the different photoinduced intramolecular electron-transfer (PET) profile. All the photophysics were rationalized by DFT calculations based on the concept of "electronic states" instead of the very often used approximation of "molecular orbitals".

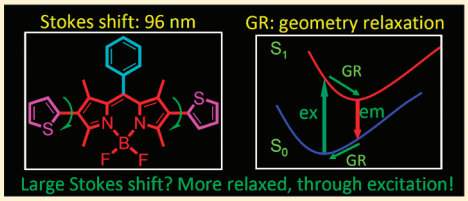

1. INTRODUCTION

Borondipyrromethenes (BODIPY) as a versatile fluorophore has attracted much attention in luminophores,[1] molecular probes or molecular logic gates,[2] light-harvesting molecular arrays,[3] photodynamic therapy (PDT),[4] and more recently, triplet−triplet annihilation (TTA) upconversions, etc.[5,6] BODIPYs are known for their robust photophysical properties, such as strong absorption of visible light (for the unsubstituted BODIPY, the molar extinction coefficient ε is up to 87000 M^{-1} cm^{-1} at 510 nm), high fluorescence quantum yield, good photostability, etc.[6a,c] Furthermore, the chemistry of BODIPY dyes is rich;[6] thus, the properties of BODIPY, such as the absorption/emission wavelength, or the hydrophilicity, etc., can be readily tuned by molecular structural modification.[1o,6,7]

The persistent and remarkable disadvantage of BODIPY dyes, that is, the small Stokes shift, has never been addressed.[6,8] A very small Stokes shift (ca. 10 nm) was usually found for BODIPY dyes.[1k,4d,6a,c,7d,9] This small Stokes shift is very often detrimental to its applications, such as in molecular probes or intracellular fluorescence imaging. A small Stokes shift reduces the emission intensity by self-absorption, or the inner filter effect.[10] Unfortunately, the typical chemical modification of the BODIPY core, i.e., extending the π-conjugation framework, which leads to red-shifted absorption and emission, is not helpful at all in increasing the Stokes shift.[1b,f,g,i,o,2h,n,4e,5b,7d−f,9,11] Although the large Stokes shift can be observed with the strategy of fluorescent-resonance-energy-transfer (FRET, Föster energy transfer), this method suffers from the drawback that self-absorption is still strong and the large Stokes shift is actually a pseudo-Stokes shift.[1i,2f,6c,11b,f,12] The inner filter effect cannot be completely eliminated by FRET if the energy acceptor shows an intrinsic small Stokes shift.[10,13]

In order to address the small Stokes shift of the BODIPY dyes, herein we devised new BODIPY derivatives that show intrinsic large Stokes shift up to 96 nm, with excitation at green (ca. 530 nm) and emission at red (ca. 620 nm). This large Stokes shift is achieved by a de novo approach, that is, to increase the *geometry relaxation* of the molecular framework upon photoexcitation. In other words, the geometry of the energy-minimized first singlet excited state, i.e., the S_1 state, which is responsible for the fluorescence (Kasha's rule), is remarkably different from the ground-state geometry (S_0 state). Therefore, the emission energy is much smaller than the excitation energy; i.e., the Stokes shift is large.[10,14] For the unsubstituted BODIPY fluorophore and the control compounds, however, we proved that the geometry of the S_1 excited state is similar to that of the S_0 state; thus the difference of the excitation energy (UV−vis absorption) and the emission energy is small; i.e., the Stokes shift is small. These analyses were supported by DFT/TDDFT calculations.

Received: November 3, 2011
Published: February 8, 2012

Scheme 1. Synthesis of the Compounds BS-1-OH, BS-1, BS-2-OH, BS-2, BS-SS, and BS-DS[a]

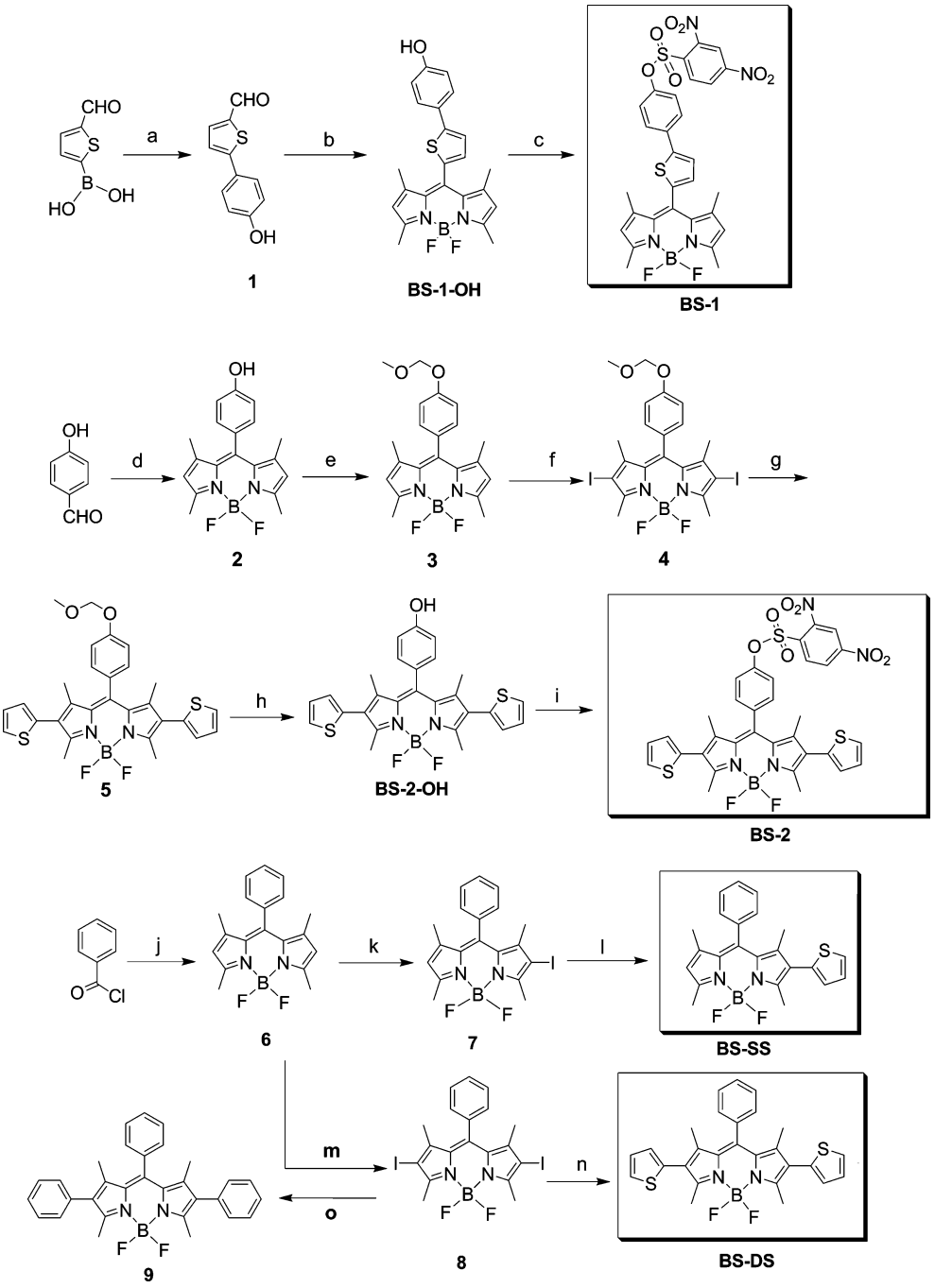

[a]Key: (a) 4-iodophenol, $K_3PO_4 \cdot 3H_2O$, $Pd(OAc)_2$, toluene, ethanol, under Ar, 80 °C, 8 h, yield 40.2%; (b) 2,4-dimethylpyrrole, TFA, THF, under Ar, overnight; DDQ, 4 h; TEA, $BF_3 \cdot OEt_2$, overnight; yield 30.0%; (c) DNBS, CH_2Cl_2, TEA, 3 h; yield 50.0%; (d) 2,4-dimethylpyrrole, TFA, THF, under Ar, overnight; DDQ, 4 h; TEA, $BF_3 \cdot OEt_2$, overnight; yield 40.0%; (e) *i*-Pr_2NEt, MOMCl, CH_2Cl_2, 60 °C; yield 50.0%; (f) NIS, CH_2Cl_2; yield 80.0%; (g) thiophene-2-boronic acid, $K_3PO_4 \cdot 3H_2O$, $Pd(OAc)_2$, toluene, ethanol, under Ar, 80 °C, 8 h; yield 67.0%; (h) 6 N HCl, EtOH, 60 °C, 4 h; yield 56.7%; (i) DNBS, CH_2Cl_2, TEA, 3 h; yield 34.0%; (j) 2,4-dimethylpyrrole, under Ar, overnight; TEA, $BF_3 \cdot OEt_2$, overnight; yield 55.0%; (k) NIS, CH_2Cl_2; yield 45.0%; (l) thiophene-2-boronic acid, $K_3PO_4 \cdot 3H_2O$, $Pd(OAc)_2$, toluene, ethanol, under Ar, 80 °C, 8 h; yield 63.4%; (m) NIS, CH_2Cl_2; yield 77.0%; (n) thiophene-2-boronic acid, $K_3PO_4 \cdot 3H_2O$, $Pd(OAc)_2$, toluene, ethanol, under Ar, 80 °C, 8 h; yield 54.4%; (o) phenylboronic acid, $K_3PO_4 \cdot 3H_2O$, $Pd(OAc)_2$, toluene, ethanol, under Ar, 80 °C, 8 h; yield 30.5%;

The increased geometry relaxation of the new BODIPY derivatives is obtained by introducing thienyl substituents at 2- and 6-position of the BODIPY core (Scheme 1). With DFT optimizations of the geometry of the S_0 and S_1 excited states, we found that the dihedral angle between the thienyl unit and the BODIPY core decreased from 55° to 39°. The new BODIPY derivatives that show large Stokes shift and red emission were used for fluorescent thiol probes, which were based on the strategy for the 2,4-dinitrobenzenesulfonyl-protected fluorophore.[2m,11j,15] Furthermore, we found that the position of the thienyl group on the BODIPY core is crucial. Substitution at the 8-position leads to a fluorophore with a small Stokes

dx.doi.org/10.1021/jo202215x | J. Org. Chem. 2012, 77, 2192–2206

shift.[6e−g] The thiol probe with this dye shows the unusual fluorescence ON−OFF switching effect, which is due to the perturbation of the normal electron transfer of DNBS thiol probes. The photophysical properties of the dyes and the probes were fully rationalized by DFT calculations. Our results are useful for design of new BODIPY derivatives that show large Stokes shifts and for applications of these dyes in molecular probes, light-harvesting molecular arrays, etc.

2. RESULTS AND DISCUSSION

2.1. Design Rationales and Synthesis of the BODIPY Derivatives. Our strategy to increase the Stokes shift is based on the Jablonski diagram; i.e., the Stokes shift is, to a large extent, dependent on the geometry relaxation of the fluorophores upon photoexcitation.[10,14] Based on the Jablonski diagram, a large Stokes shift will be produced by large *geometry relaxation*; i.e., the geometry difference between the S_0 state and the S_1 state. For the unsubstituted BODIPY fluorophore, the molecular framework is rigid; thus, small geometry relaxation and small Stokes shifts are expected. With thienyl substitution at the 2- and 6-positions, the molecular flexibility was increased; that is, the dihedral angle between the thienyl and the BODIPY core may be changed upon excitation. This enhanced geometry relaxation will increase the Stokes shift.[10,14] The experimental results fully proved our postulations.

The synthesis of the compounds is straightforward (Scheme 1). With iodination of the BODIPY core by *N*-iodosuccinimide (NIS), monoiodo- or bisiodo-BODIPY (**BS-SS** or **BS-DS**) were obtained. Then the monothienyl- or bis-thienyl-substituted derivatives **BS-SS** and **BS-DS** were obtained by using Pd(0)-catalyzed Suzuki cross-coupling reactions with 2-thienyl boronic acid (Scheme 1). In order to use this BODIPY derivatives to construct a fluorescent thiol probe, we prepared 8-(4′-hydroxyl)phenyl-substituted 2,6-bisthienyl derivatives **BS-2-OH**. Since we found that direct iodination of compound **2** leads to a complicated mixture, the phenolic group was protected with methyl chloromethyl ether (MOMCl) prior to iodination with NIS (Scheme 1). After the bis-iodination of BODIPY, the protection MOM was readily removed by treatment with half-concentrated HCl acid under mild conditions (Scheme 1). Then the thiol probe **BS-2** was obtained by reaction of **BS-2-OH** with 2,4-dinitrobenzenesulfonyl chloride (DNBS-Cl). All of the compounds were obtained in moderate to satisfying yields (see the Experimental Section for details). Compound **9** was prepared as a control compound to study the different effects of the phenyl and thienyl substituents (**BS-DS**) on Stokes shifts.

We also prepared a control compound with the thienyl substituent at the 8-position (**BS-1-OH**, Scheme 1) to study the effect of substitution position of the thienyl moiety on the photophysical properties. The 4′-hydroxylphenyl group at the 5-position of the thienyl moiety is for preparation of the thiol probe **BS-1** (Scheme 1). Direct preparation of BODIPY derivatives with 2-formyl thienyl was unsuccessful. **BS-2** is a fluorescence OFF−ON thiol probe, but interestingly, **BS-1** is a fluorescence ON−OFF probe. That is, the compound **BS-2-OH** is fluorescent and probe **BS-2** is nonfluorescent. For dye **BS-1-OH** and the probe **BS-1**, however, the emissive profile is reversed; i.e., **BS-1-OH** is nonfluorescent but probe **BS-1** is fluorescent. These fluorescence relays can be rationalized by different photoinduced electron transfer processes of the compounds, which is supported by the DFT and TDDFT calculations.

2.2. UV−vis Absorption of the Thienyl-BODIPY Fluorophores. The UV−vis absorption of the compounds were studied (Figure 1). Compared to the unsubstituted

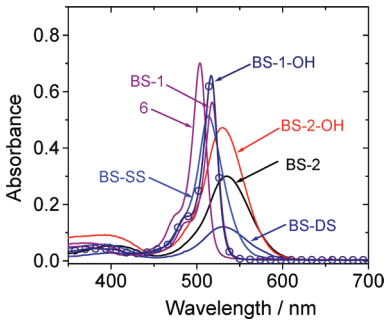

Figure 1. UV−vis absorption spectra of the compounds (in toluene); 7.5×10^{-6} M, 25 °C.

BODIPY,[6a−d] the new derivatives show red-shifted absorption. For example, **BS-SS** shows absorption at 514 nm, and the bisthienyl-substituted derivative **BS-DS** gives absorption at 529 nm. These red-shifted absorptions are due to the slightly extended π-conjugation framework, which was proved by the DFT calculations (discussed later). For the derivatives with a thienyl substituent at 8-position (**BS-1** and **BS-1-OH**), however, the absorption/emission wavelengths do not show significant red-shifts. DFT calculations indicate that in this case the thienyl is not involved in the frontier molecular orbitals; i.e. the π-conjugation framework is not extended to the thienyl moiety (Supporting Information). The control compound with phenyl moieties at the 2,6-position was prepared (**9** in Scheme 1). Compound **9** shows similar red-shifted absorption at 530 nm compared to the unsubstituted BODIPY (compound **6**) at 504 nm (Supporting Information).

We noticed that the derivatives with thienyl substitution at the 8-position of BODIPY core gave a similar absorption wavelength. For example, **BS-1** (with thienyl moiety at the meso-position) gives absorption maxima at 514 nm.

2.3. Emission of the New Derivatives with Large Stokes Shifts. The fluorescence of the new derivatives was studied (Figure 2). For the unsubstituted BODIPY (**6**), the typical small Stokes shift (10 nm) was observed (Figure 2c), with the excitation and emission maxima at 506 and 516 nm, respectively. Interestingly, much larger Stokes shift were observed for the new derivatives with the thienyl moiety at 2- or 2,6-position of the BODIPY core. For example, excitation and emission maxima of compound **BS-SS** at 509 and 601 nm were observed, respectively (Figure 2a). Thu, the Stokes shift is up to 92 nm. To the best of our knowledge, this is among the largest Stokes shifts ever reported for the BODIPY dyes, without resorting to the FRET effect, etc.[1i,6a,c]

Interestingly, with thienyl substitution at the 8-position, no large Stokes shift was observed. For example, the excitation and emission maxima of **BS-1** are at 515 and 527 nm, respectively. Thus, the Stokes shift of **BS-1** is 12 nm (see Figure 12). This small Stokes shift is typical for BODIPY dyes.[2a,b,6,11b,g,15f,16] A similar emission profile was found for **BS-1-OH** (Supporting Information).

We noticed that BODIPY derivatives with thienyl units at the 3- or 3,5-positions were reported.[11e,17] However, those compounds show a typical small Stokes shift of BODIPY (17−29 nm), although the emission wavelengths are red-shifted

dx.doi.org/10.1021/jo202215x | J. Org. Chem. 2012, 77, 2192−2206

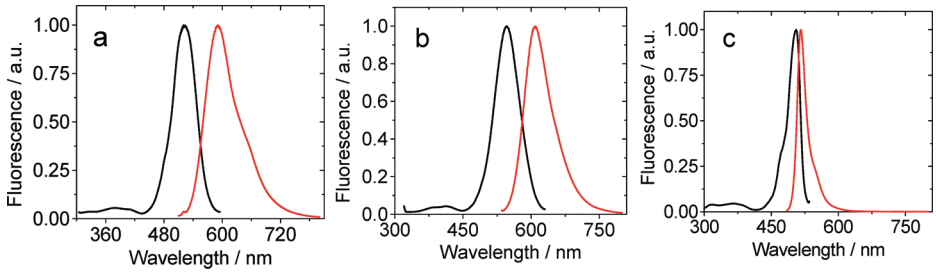

Figure 2. Emission and excitation spectra of (a) **BS-SS** (λ_{ex} = 520 nm, λ_{em} = 600 nm); (b) **BS-DS** (λ_{ex} = 530 nm, λ_{em} = 636 nm); and (c) compound **6** (unsubstituted BODIPY) (λ_{ex} = 480 nm, λ_{em} = 536 nm). The wavelengths were used for measuring the excitation/emission spectra, they are not the excitation/emission maxima. $c = 7.5 \times 10^{-6}$ M in toluene, 25 °C.

(587−643 nm) compared to the unsubstituted BODIPY dyes. It is clear that red-shifted emission does not necessarily induce a large Stokes shift because the two photophysical parameters are of entirely different origin.[10,14] It should be pointed out that the red-shifted absorption and emission of the new BODIPY derivatives are not due to the electron-donating capability of the moiety at the 8-position of the BODIPY core because previously blue-shifted absorption and emission were observed with amino or 4-hydroxylphenyl substituents at the 8-position.[18,2l] Also, the Stokes shift of the BODIPY cannot be increased by extension of the π-conjugation at the 2,6-postions, such as with C≡C triple bonds.[2m,7a,11h,k,19]

In principle, the emission wavelength of fluorophore is related to the size of π-conjugation framework, or the intramolecular charge transfer (ICT) feature of the fluorophore.[1g] For the Stokes shift, however, the geometry relaxation at the S_1 state after vertical excitation from S_0 state is crucial (from the Franck−Condon excited state to the energy-minimized geometry at the S_1 state).[10,14] It should be pointed out that no geometry changes occur during the excitation process (vertical excitation, Franck−Condon principle).[10,14] The geometry relaxation only occurs after the vertical excitation, i.e., at the S_1 state before decay $S_1 \rightarrow S_0$. In a later section, we will show that with increased geometry relaxation at the S_1 state the Stokes shift of the fluorophore will increase. This is true for **BS-SS**, **BS-DS**, etc. For the dyes with thienyl moieties at the 3- or 8-position, however, the geometry changes are smaller; thus the Stokes shifts of these dyes are small. This is obvious from the Jablonski diagram (Figure 6 and Supporting Information).[10,14]

The control compound **9** shows emission maxima at 555 nm, which is red-shifted from the thienyl-substituted compounds **BS-DS** and **BS-SS**. However, the Stokes shift of compound **9** is only 26 nm (Table 1 and Supporting Information).

We found that the UV−vis absorption of BODIPY derivatives are not sensitive to solvent polarity (Figure 3a). Interestingly, the emission wavelength of **BS-DS** is independent of the solvent polarity (Figure 3b), although the emission intensity decreased in more polar solvents, such as methanol, than that in nonpolar solvents, such as toluene. This result indicates that the large Stokes shift of the new BODIPY derivatives is intrinsic property, not a solvent-polarity induced phenomena, or any intramolecular charge transfer (ICT) related result.[10]

The absorption and emission changes of BODIPY dyes with thienyl substitution are clearly visible (Figure 4). For example, the solution of the unsubstituted BODIPY gives light green color. For the thienyl substituted BODIPY derivatives, however, purple color was observed. The emission changed from green to red. The red-shifted absorption and emission of the BODIPY derivatives, especially the large Stokes shift, will be useful for the application of the dyes in fluorescent molecular probes or intracellular fluorescent bioimagings.[2k,3c] Previously the thienyl substituted BODIPY derivatives (at the 2−6 position) were reported, but the photophysical properties were not studied in detail.[20]

2.4. Rationalization of the Large Stokes Shift of the Thienyl-Substituted BODIPYs with DFT Calculations: Geometry Relaxation upon Photoexcitation. In order to rationalize the photophysical properties of the new derivatives, such as the UV−vis absorption and fluorescence, especially the *large* Stokes shift, the geometry of the molecules at the ground state (S_0 state) and the S_1 excited state was optimized by density functional theory (DFT) and time-dependent DFT (TDDFT) methods. The energy gap between the S_0 state and the S_1 excited state (excitation energy) was calculated with the TDDFT method based on the optimized S_0 state geometry (for absorption) and the S_1 state geometry (for fluorescence), respectively. Revealing the photophysical properties from a theoretical perspective will be useful for the design of new fluorophores.

First the ground state (S_0) geometry of **BS-DS** was optimized (for the molecular structure please refer to Figure 5). The dihedral angle between the thienyl and BODIPY moiety is 55°. However, HOMO is spread over both the BODIPY and the thienyl moiety, indicating that the π-conjugation between the thienyl moiety and the BODIPY core is remarkable even when the two moieties are not fully coplanar. It is known that thienyl is an efficient π-conjugation linker and has been widely used in organic chromophores such as those for dye-sensitized solar cells.[21] On the basis of the optimized S_0 state geometry, the vertical excitation (UV−vis absorption) was calculated with the TDDFT method. The calculated absorption bands are located at 488 and 395 nm (Figure 5), which are in agreement with the experimental results of 521 and 394 nm (**BS-DS**) (Figure 1). These two absorption bands can be assigned to the $S_0 \rightarrow S_1$ and $S_0 \rightarrow S_3$ transitions, respectively (Table 2). Similar calculations were carried out for other dyes (Table 2).

In order to study the emission, the S_1 state geometry was optimized.[10,14] The energy gap between the S_0 state and S_1 state, calculated with the optimized S_1 state geometry, is the fluorescence emission wavelength.[10,14] The most prominent difference between the S_0 state geometry and the energy-minimized geometry of S_1 state is the dihedral angle between the BODIPY core and the thienyl moiety. Compared to the dihedral angle at S_0 state geometry (55°), the two moieties become more coplanar at the optimized S_1 excited state, for which the dihedral angle is 39°. This geometry relaxation upon photoexcitation imparts remarkable effect on the energy level of the molecular orbitals. For example, the LUMO is stabilized by 0.17 eV at the S_1 state geometry compared to that at the S_0 state geometry, but the HOMO is destabilized by 0.24 eV for S_1

dx.doi.org/10.1021/jo202215x | J. Org. Chem. 2012, 77, 2192−2206

Table 1. Photophysical Parameters of the Compounds

compds	solvents	λ_{abs} [a] (nm)	λ_{em} [b] (nm)	$\Delta\nu$ [c] (nm)	ε [d] (M^{-1} cm^{-1})	Φ_F [e] (%)	τ [f] (ns)
BS-2	$PhCH_3$	535	608	73	40000	5.9	3.6
	DCM	533	607	74	42000	*g*	*g*
	CH_3OH	526	609	83	41000	*g*	*g*
	CH_3OH/H_2O =4/1	527	619	92	41000	0.7	*g*
BS-2-OH	$PhCH_3$	530	604	74	63000	57.3	3.8
	DCM	528	605	77	62000	*g*	*g*
	CH_3OH	521	602	81	59000	*g*	*g*
	CH_3OH/H_2O =4/1	522	609	87	59000	8.8	*g*
BS-DS	$PhCH_3$	530	609	79	16000	47.2	3.4
	DCM	527	609	82	16000	*g*	*g*
	CH_3OH	521	610	89	17000	*g*	*g*
	CH_3OH/H_2O =4/1	523	612	89	17000	5.1	*g*
BS-SS	$PhCH_3$	513	591	78	69000	20.6	3.2
	DCM	511	594	83	66000	*g*	*g*
	CH_3OH	507	600	93	65000	*g*	*g*
	CH_3OH/H_2O =4/1	507	603	96	65000	3.2	*g*
6	$PhCH_3$	504	516	12	94000	85.2	3.4
	DCM	501	513	12	87000	*g*	*g*
	CH_3OH	498	509	11	88000	*g*	*g*
	CH_3OH/H_2O =4/1	501	509	8	86000	*g*	3.7
BS-1	$PhCH_3$	518	530	12	75000	6.6	*g*
	DCM	515	528	13	79000	*g*	*g*
	CH_3OH	512	523	11	71000	*g*	*g*
	DMF/H_2O =4/1	514	528	14	69000	5.4	*g*
BS-1-OH	$PHCH_3$	517	528	11	88000	6.9	3.5
	DCM	514	525	11	90000	*g*	*g*
	CH_3OH	511	521	10	82000	*g*	*g*
	DMF/H_2O =4/1	514	*g*	*g*	73000	0.4	*g*
9	$PhCH_3$	530	556	26	26000	32.5	4.1
	DCM	528	555	27	40000	*g*	*g*
	CH_3OH	524	550	26	9000	*g*	*g*
	CH_3OH/H_2O =4/1	524	551	27	10000	*g*	*g*

[a] λ_{abs} (nm): absorption wavelength of first absorption maximum. [b] λ_{em} (nm): emission wavelength (at the maximum intensity). [c] $\Delta\nu$: Stokes shifts. [d] ε: extinction coefficient. [e] Φ: fluorescence quantum yields, with unsubstituted BODIPY (compound **6**) as the standard (Φ = 72.0% in tetrahydrofuran). [f] τ (ns): fluorescence lifetimes. [g] Not determined.

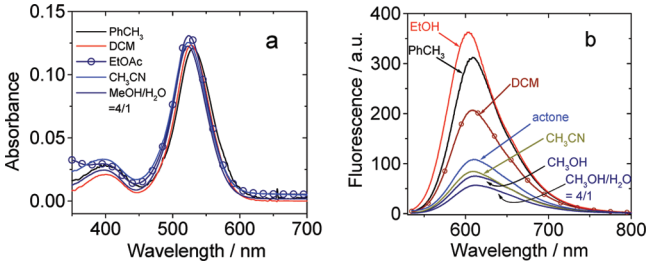

Figure 3. (a) UV–vis absorption spectra of **BS-DS** in different solvents. (b) Fluorescence spectra of **BS-DS** in different solvents. c = 7.5 × 10^{-6} M. λ_{ex} = 530 nm. 25 °C.

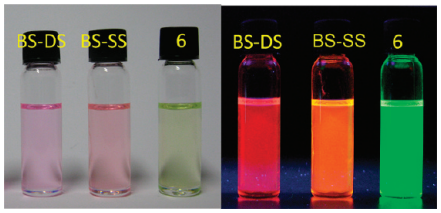

Figure 4. Fluorescence photographs of the compounds, taken under ambient light and UV light (hand-held UV lamp, 365 nm). c = 7.5 × 10^{-6} M. In toluene. 25 °C.

state geometry compared to that at the S_0 state geometry. As a result, the energy gap between the HOMO and LUMO is greatly *decreased* with geometry relaxation at the S_1 state compared to that at S_0 state geometry (UV–vis absorption, i.e., excitation). We propose this *geometry relaxation* is the main origin of large Stokes shift for **BS-DS**, which is in agreement with the Jablonski diagram of the fluorescence.[10] The fluorescence wavelength was calculated as 625 nm (in methanol), which is in very good agreement with the experimental result of 610 nm (Figure 2).

We noticed that BODIPY derivatives with thienyl substituents at the 2,6-position have been reported, but the origin of the large Stokes shift was not discussed.[20] Our rationalization of the Stokes shift by the concept of geometry relaxation at the S_1 state, supported by the DFT calculations, will be useful for design of fluorophores that show large Stokes shift. To the best of our knowledge, this rationale has never been used for design of fluorophores to access large Stokes shifts.

With the thienyl substituent at the 8-position, the derivative **BS-1** gives the typical small Stokes shift of 12 nm (Table 1). Our later study shows that for **BS-1** the thienyl moiety is not involved in the frontier molecular orbitals of the electronic

dx.doi.org/10.1021/jo202215x | J. Org. Chem. 2012, 77, 2192–2206

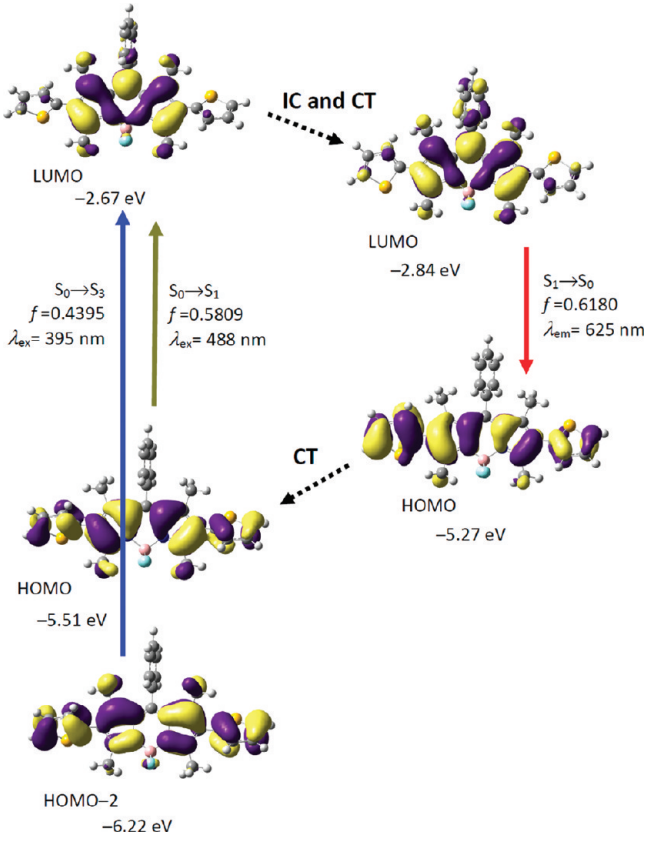

Figure 5. Rationalization of the large Stokes shift of **BS-DS**: the geometry relaxation upon photoexcitation and the frontier molecular orbitals (MOs) involved in the vertical excitation (i.e., UV−vis absorption, the left two columns) and emission (right column) of **BS-DS**. The vertical excitations were calculated based on the optimized ground state geometry (S_0), the emission was calculated based on the optimized geometry of the excited state (S_1). Methanol was used as the solvent (PCM model). Calculated at B3LYP/6-31G(d)/level using Gaussian 09W. Note the energy levels of HOMO and LUMO at S_1 state are different from that at S_0 state. IC stands for internal conversion and CT stands for conformation transformation. Excitation and radiative processes are marked as solid lines and the nonradiative processes are marked by dotted lines.

transitions. Furthermore, the geometric relaxation of **BS-1** at the singlet excited state (S_1 state) is very small. For example, the dihedral angle between the thienyl substituent and the BODIPY core shows a very small change of 2°, with dihedral angles of 89° and 87° for the optimized S_0 state geometry and the optimized S_1 state geometry, respectively. By comparison, the compound **BS-2**, which gives a large Stokes shift of 92 nm, shows a dihedral angle change (geometry relaxation) of 16°. Furthermore, the substantial changes of the energy levels of the molecular orbitals and the excited state contributed to the Stokes shifts. A rigid fluorophore, without geometry relaxation upon photoexcitation, will give a small Stokes shift.[10,14] It should be pointed out that the Stokes shift of BODIPYs were rarely studied by the DFT calculations.[22]

We noticed that BODIPY derivatives with thienyl substitutions at the 3- or 3,5-positions have been reported to give red-shifted emission in the region 587−643 nm. However, the Stokes shifts of those BODIPY derivatives are 17−29 nm,[11e] much smaller than the Stokes shift of the current BODIPY derivatives with thienyl substituents at the 2- or 2,6-positions, such as **BS-SS**, **BS-DS** and **BS-SS** (Stokes shift is up to 96 nm). We also investigated the geometrical relaxation of BODIPY derivatives with 3,5-thienyl substituents that give smaller Stokes shift (see the Supporting Information); the results indicate that those compounds give smaller dihedral angle changes (less than 10°).[11e] Previously, BODIPY derivatives with aryl substituents at the 3,5-position were prepared to show relatively large Stokes shifts (up to 65 nm),[23] but the origin of the large Stokes shift was not rationalized.

The geometry changes of the control compound **9**, with phenyl groups at the 2- and 6-positions, which show a small Stokes shift of ca. 20 nm, was also studied with the DFT calculations (Supporting Information). Although the dihedral angles varied significantly upon excitation, the energy levels of the molecular orbitals gave very small changes, which resulted in a small Stokes shift for **9** (Supporting Information). This theoretical approach to rationalize the Stokes shift is applicable to the 8-(2-furyl) BODIPY or the 8-(2-thienyl) BODIPY,[6f] which are known with relative large Stokes shift (see the Supporting Information for the detailed calculation results).

Table 2. Selected Parameters for the Vertical Excitation (UV−vis Absorptions) and Emission of BS-DS and BS-SS; Electronic Excitation Energies (eV) and Oscillator Strengths (*f*), Configurations of the Low-Lying Excited States of the Compounds (Methanol Used as Solvent in All of the Calculations, Calculated at the DFT/TDDFT//B3LYP/6-31G(d) Level with Gaussian 09W)

			TDDFT//B3LYP/6-31G(d)			
compd		electronic transitions[a]	excitation energy	f[b]	composition[c]	CI[d]
BS-DS	absorption[e]	$S_0 \rightarrow S_1$	2.54 eV (488 nm)	0.5809	H-2→L	0.2219
					H→L	0.6714
		$S_0 \rightarrow S_3$	3.14 eV (395 nm)	0.4395	H-2→L	0.6673
					H→L	−0.2255
	emission[f]	$S_1 \rightarrow S_0$	1.98 eV (625 nm)	0.6180	H→L	0.7031
BS-SS	absorption[e]	$S_0 \rightarrow S_1$	2.68 eV (462 nm)	0.4755	H-1→L	0.2659
					H→ L	0.6538
		$S_0 \rightarrow S_2$	3.13 eV (396 nm)	0.3460	H-1→L	0.6517
					H→L	0.2709
	emission[f]	$S_1 \rightarrow S_0$	2.01 eV (616 nm)	0.4292	H→L	0.7027

[a]Only selected excited states were considered. The numbers in parentheses are the excitation energy in wavelength. [b]Oscillator strength. [c]H stands for HOMO and L stands for LUMO. Only the main configurations are presented. [d]Coefficient of the wave function for each excitations. The CI coefficients are in absolute values. [e]The calculations on UV−vis absorption were based on the optimized ground-state geometry. [f]The calculations on fluorescence are based on the optimized S_1 state geometry.

dx.doi.org/10.1021/jo202215x | J. Org. Chem. 2012, 77, 2192−2206

The origin of the Stokes shifts of fluorophores can be illustrated by the simplified Jablonski diagram in Figure 6.[10,14] Large

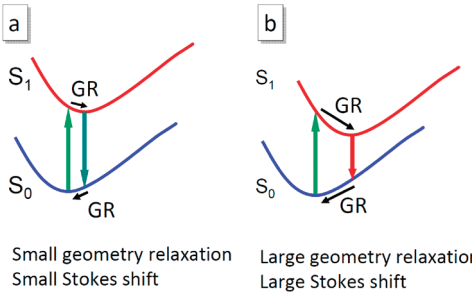

Figure 6. Simplified Jablonski diagram for the origin of the Stokes shifts of thienyl-substituted BODIPYs. (a) Small geometry relaxation upon photoexcitation produces small Stokes shift, which is applicable to the unsubstituted BODIPY fluorophore and **BS-1**. (b) Large geometry relaxation upon photoexcitation leads to large Stokes shift, which is applicable to **BS-2**, **BS-DS**, and **BS-SS**. GR stands for geometry relaxation.

geometry relaxation at the excited state (S_1 state) and the change of the energy levels of the electronic states along with the geometry relaxation will produce large Stokes shift. Conversely, small geometry relaxation at the excited state will produce a small Stokes shift. The geometry relaxation is the geometry difference between the energy-minimized S_0 state and the energy-minimized S_1 state, which can be predicted by the DFT and the TDDFT calculations. This de novo approach to access the large Stokes shift of a fluorophore by introduce of remarkable geometry relaxation at the S_1 excited state will be useful for design of new fluorophores that show large Stokes shifts. This remains a challenge for chemists.

2.5. Application of the New BODIPY Derivatives for Fluorescent Thiol Probe. Fluorophores with large Stokes shift and long emission wavelength are ideal for applications in fluorescent molecular probes because of the elimination of the inner filter effect, etc.[10,14] Thus, the new **BODIPY** derivatives described herein (**BS-SS** and **BS-DS**, Scheme 1) are ideal for construction of molecular probes. Detection of thiols with fluorescent molecular probes have attracted much attention.[24] DNBS-protected fluorophore is a straightforward strategy for construction of fluorescent OFF−ON switching thiol probes.[2l,15a,b,d,e,24e,25] Previously, we prepared fluorescent thiol probes with pyrene, BODIPY, and styryl-BODIPY as the fluorophores, and fluorescence OFF−ON switching effect was achieved.[11j,15c,f] With DFT/TDDFT calculations, we proposed that the fluorescence OFF feature of this kind of thiol probes is caused by the *dark excited states* of the probes, whereas the fluorescence switching-ON effect in the presence of thiols is caused by the *emissive* S_1 excited state of the cleavaged product (the released free fluorophore).[11j,15c,f] Thus, the photophysical properties of the probes can be rationalized by the concept of "electronic state" instead of the very often used approximation of "molecular orbitals". Herein we devised the thiol probe **BS-2** to explore the new fluorophores that show large Stokes shift for construction of fluorescent thiol probes.

First, the UV−vis absorption of **BS-2** was studied (Figure 7). In the presence of thiols such as cysteine, the absorption of **BS-2** at 527 nm was enhanced. This is in line with the stronger absorption of the free fluorophore **BS-2-OH** at 522 nm

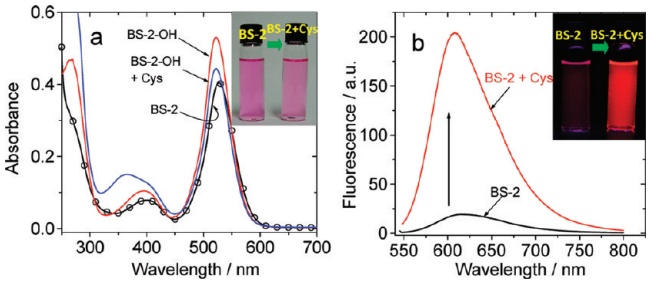

Figure 7. UV−vis absorption of **BS-2** (1.0×10^{-5} M) before and after treatment with **Cys** (200 equiv) for 20 min. 25 °C. (b) Fluorescence spectral changes of probe **BS-2** (1.0×10^{-5} M) before and after treating with 200 equiv of Cys. λ_{ex} = 540 nm. In mixed solvent MeOH/H_2O (4:1, v/v). 37 °C.

(ε = 59000 M^{-1} cm^{-1}) vs the probe **BS-2** at 527 nm (ε = 41000 M^{-1} cm^{-1}).

The probe **BS-2** gives a weak emission at 619 nm. In the presence of cysteine, however, the emission intensity was enhanced 11-fold (Figure 7b). The sensing mechanism of probe **BS-2** is the cleavage of the DNBS moiety by the thiols, thus the release of the free fluorophore **BS-2-OH**.[11j,15a−c,f,24e]

The ideal fluorescent probes will be those that show pH-independent fluorescence transduction.[16b] Thus, the pH-dependency of the emission of fluorophore **BS-2-OH** was studied (Figure 8a). For **BS-2**, the background emission is weak

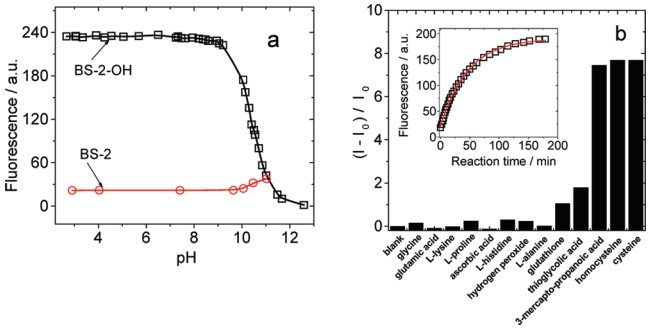

Figure 8. (a) Fluorescence response of **BS-2** and **BS-2-OH** (1.0×10^{-5} M) to different pH. (b) Fluorescence response of **BS-2** (1.0×10^{-5} M) before and after incubation with 200 equiv of different analytes for 180 min. Inset of (b): reaction kinetic of **BS-2** (1.0×10^{-5} M) with 200 equiv of Cys. λ_{ex} = 540 nm. λ_{em} = 608 nm. In MeOH/water (4/1, v/v). 37 °C.

in the range of pH 3.0−10.0. The emission increased slightly at high pH range, probably because of the hydrolysis of the sulfonic ester at basic conditions. The emission is stable in a wide range of pH 3.0−10.0, which is sufficient for in vivo fluorescence imaging studies.

The selectivity of **BS-2** toward different biologically related analytes was studied (Figure 8b). The probe gives a similar response to thiols with small molecular size, such as cysteine, homocysteine, and 3-mercaptopropanoic acid. No response was found for other analytes, such as glycine or lysine, etc. Thus, the probe **BS-2** is selective toward thiols and has good immunity toward biologically related neucleophiles.[2l,11j,15,24e] It should be pointed out that the probe does not show any selectivity between different small molecular thiols, such as cysteine, homocysteine, or 3-mercaptopropanoic acid; however, this is expected because of the specific sensing mechanism.[2l,11j,15,24e]

dx.doi.org/10.1021/jo202215x | J. Org. Chem. 2012, 77, 2192−2206

Probe **BS-2** was used for fluorescent imaging of intracellular thiols (Figure 9). With excitation at 543 nm, red emission was observed. *N*-Methylmaleimide was used as control to demonstrate that the emission observed is due to the presence of intracellular thiols.

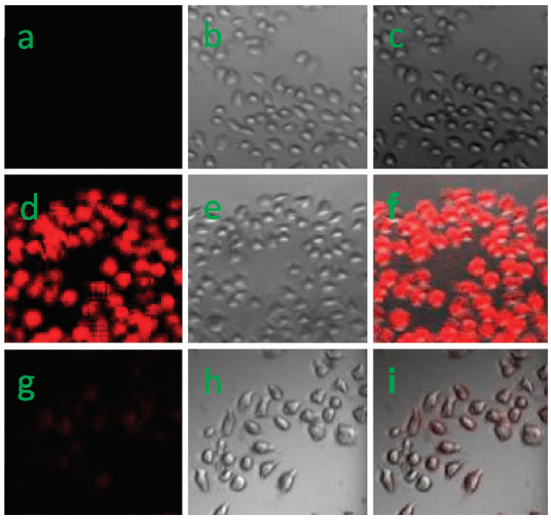

Figure 9. Fluorescence images of Hela cells. (a) Fluorescence image of cells in the absence of probe **BS-2**; (d) fluorescence image of cells incubated with probe **BS-2** (20 μM) for 45 min; (g) fluorescence image of cells pretreated with *N*-methylmaleimide (0.5 mM, to remove the intracellular thiols) for 1 h and then incubated with probe **BS-2** (20 μM) for 45 min; (b, e, h) corresponding bright field images of (a, d, g); (c, f, i) overlays of the fluorescent and bright field images. λ_{ex} = 543 nm. 37 °C.

2.6. DFT/TDDFT Calculations: Rationalization of the Fluorescence OFF−ON Effect of the Thiol Probe BS-2. In recent years, fluorescent molecular probes have been investigated extensively.[26,24e] However, the fluorescence transduction of the probes, such as the fluorescence OFF−ON switching effect, were rarely studied from a point of view of theoretical chemistry, such as by using DFT calculations.[27] Recently, we studied the fluorescence OFF−ON switching effect of the DNBS-based thiol probes.[11j,15c,f] We and others used the concept of "electronic state", instead of the "molecular orbitals" (such as HOMO and LUMO), to rationalize the photophysical properties of the molecular porbes.[11j,15c,f,27c] We proposed that the fluorescence OFF state of the probes is due to the dark excited state of the probes, that is, the S_1 state is nonemissive, which is deduced from the oscillator strength of the $S_0 \rightarrow S_1$ transition and the molecular orbitals involved in the transition (usually an electron transfer process, leading to a transition integer to be zero, makes the $S_0 \rightarrow S_1$ transition a forbidden transition). $S_1 \rightarrow S_0$ will follow the same rule; thus, the probe is nonfluorescent.[11j,15c,f] The fluorescence switching ON effect of the thiol probes in the presence of thiols is due to the cleavage of the DNBS moiety off the fluorophore, thus the dark excited state was removed, the S_1 state of the free fluorophore is emissive, and the fluorescence of the fluorophore is switched on. All these rationalizations are based on DFT and TDDFT calculations.[11j,15c,f] Clearly, more examples are required to confirm this concept.

The UV−vis absorption and the emission properties of **BS-2** were studied with DFT calculations. First, the ground-state geometry was optimized and the UV−vis absorption was calculated by the TDDFT method based on the ground-state geometry (vertical excitation, Franck−Condon principle). The components of the transitions are listed in Table 3, and the frontier molecular orbitals involved in the transitions are presented in Figure 10.

We observed two main absorption bands for **BS-2** with the calculations, transitions of $S_0 \rightarrow S_4$ and $S_0 \rightarrow S_9$), which are located at 492 and 398 nm, respectively. These calculated absorption bands are in good agreement with experimental results (527 and 401 nm, Figure 7). The $S_0 \rightarrow S_1$ transition of the **BS-2** is a forbidden transition. The molecular orbitals that are involved in the transition are HOMO→LUMO, which

Table 3. Selected Parameters for the Vertical Excitation (UV−vis Absorptions) and the Emission of Thiol Probe BS-2 and BS-2-OH; Electronic Excitation Energies (eV) and Oscillator Strengths (f), Configurations of the Low-Lying Excited States of the Compounds; Calculation of the S_0−S_1 Energy Gaps Based on Optimized Ground-State Geometries (UV-vis Absorption) and the Optimized Excited-State Geometries (Fluorescence Emission) (Methanol Used as Solvent, Calculated at TDDFT//B3LYP/6-31G(d) Level with Gaussian 09W)

			TDDFT//B3LYP/6-31G(d)			
compd		electronic transitions[a]	excitation energy	f[b]	composition[c]	CI[d]
BS-2-OH	absorption[e]	$S_0 \rightarrow S_1$	2.54 eV (489 nm)	0.5846	H-2→L	0.2167
					H→L	0.6731
		$S_0 \rightarrow S_4$	3.14 eV (395 nm)	0.4322	H-2→L	0.6690
					H→L	0.2202
	emission[f]	$S_1 \rightarrow S_0$	2.00 eV (620 nm)	0.6154	H→L	0.7031
BS-2	absorption[e]	$S_0 \rightarrow S_1$	1.84 eV (675 nm)	0.0001	H→L	0.7061
		$S_0 \rightarrow S_4$	2.52 eV (492 nm)	0.5611	H-2→L+2	0.2253
					H→L+2	0.6690
		$S_0 \rightarrow S_9$	3.12 eV (398 nm)	0.4369	H-2→L+2	0.6660
					H→L+2	0.2289
	emission[f]	$S_1 \rightarrow S_0$	0.92 eV (1353 nm)	0.0002	H→L	0.7067
		$S_5 \rightarrow S_0$[g]	2.18 eV (569 nm)	0.8694	H→L+2	0.7033

[a]Only selected excited states were considered. The numbers in parentheses are the excitation energy in wavelength. [b]Oscillator strength. [c]H stands for HOMO and L stands for LUMO. Only the main configurations are presented. [d]Coefficient of the wave function for each excitations. The CI coefficients are in absolute values. [e]The calculations on UV−vis absorption are based on the optimized ground-state geometry. [f]The calculations on fluorescence emissions are based on the optimized S_1 state geometry. [g]The emission was calculated at the optimized S_5 state geometry.

dx.doi.org/10.1021/jo202215x | J. Org. Chem. 2012, 77, 2192−2206

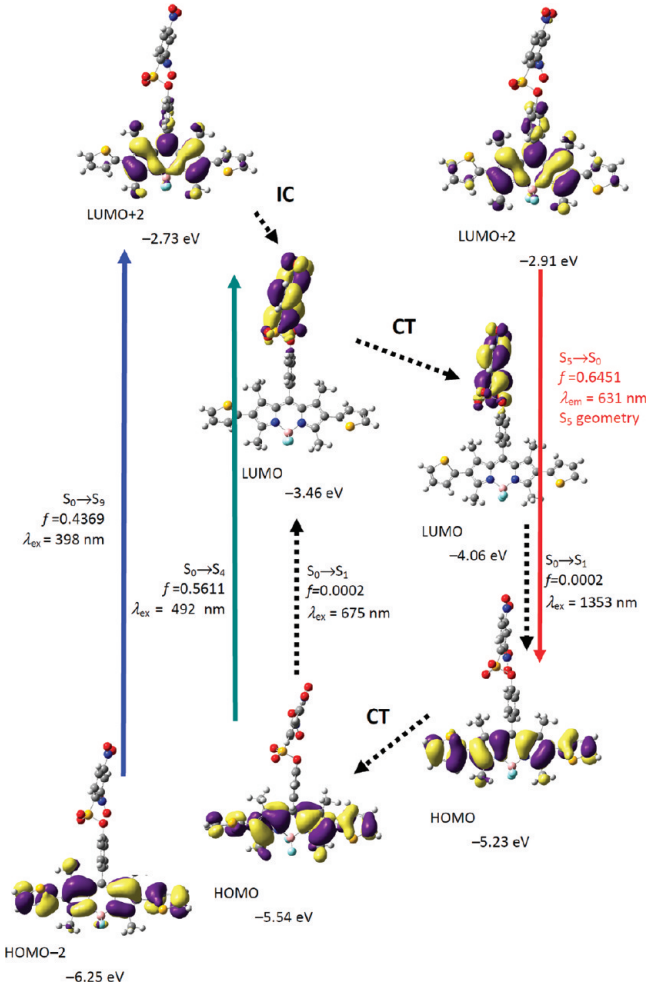

Figure 10. Rationalization of the UV−vis absorption and the weak emission of **BS-2**: the frontier molecular orbitals (MOs) involved in the vertical excitation (i.e., UV−vis absorption, the left two columns) and emission (the right column). Methanol was used as the solvent for the calculations (PCM model). The vertical excitation related calculations are based on the optimized ground state geometry (S_0), the emission related calculations were based on the optimized excited state (S_1), at the B3LYP/6-31G(d)/level using Gaussian 09W. Note the energy levels of the HOMO and LUMO at S_1 state are different from that at the S_0 state. IC stands for internal conversion and CT stand for conformation transformation. Excitation and radiative decay processes are marked as solid lines and the nonradiative processes are marked by dotted lines.

indicated a complete electron transfer (Figure 10). The calculated absorption band is at 675 nm. Experimentally, we did not observe this absorption band in the UV−vis absorption spectra (Figure 7).

In order to study the emission of **BS-2**, the geometry of S_1 excited state was optimized and the emission was calculated with the TDDFT method (usually S_1 state is responsible for the fluorescence, Kasha's role) (Table 3). We found that S_1 state is a dark state (f = 0.0001), that is, the $S_1 \rightarrow S_0$ is most probably a forbidden transition. The calculated energy gap between the S_0 state and the S_1 state is 1353 nm. This dark excited state is responsible for the experimentally observed weak emission of probe **BS-2**.

However, emission at 619 nm was observed for **BS-2**. In order to rationalize this emission band, we examined the higher excited state of probe **BS-2**. We found that $S_5 \rightarrow S_0$ transition is most probably responsible for the emission of probe **BS-2** at 619 nm (the calculated emission wavelength is 631 nm with optimized S_5 state geometry). Emission from higher excited state other than the S_1 state usually is weak, especially with the S_1 state as a dark excited state because the nonemissive internal conversion (IC) is competitive to the radiative decay process of $S_5 \rightarrow S_0$.[10b,14]

In the presence of thiols (such as cysteine), the emission of probe is switched on after cleavage of the DNBS moiety (which is a strong intramolecular electron trap) (Figure 7). In order to rationalize this fluorescence switching ON effect, the UV−vis absorption and the fluorescence of the released fluorophore were also studied with the DFT/TDDFT calculations (Figure 11 and Table 3).

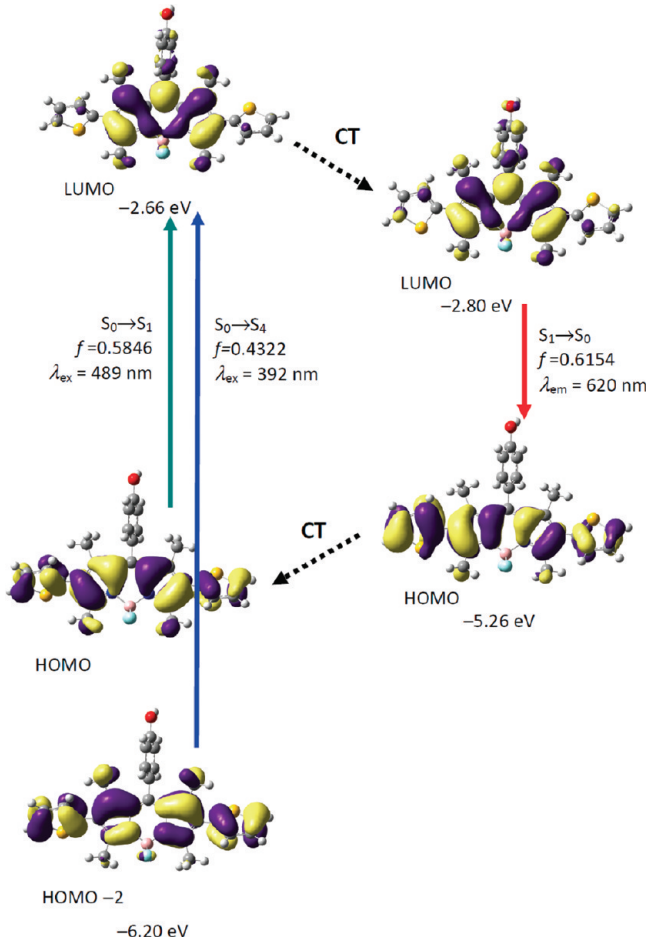

Figure 11. Rationalization of the UV−vis absorption, strong emission and the large Stokes shift of **BS-2-OH**: the geometry relaxation and the frontier molecular orbitals (MOs) involved in the vertical excitation (i.e., UV−vis absorption, the left two columns) and emission (the right column) of **BS-2-OH**. The vertical excitation related calculations are based on the optimized geometry of the ground state (S_0), the emission related calculations were based on the optimized geometry of the excited state (S_1). Methanol was used as solvent for the DFT calculations. At the B3LYP/6-31G(d)/level using Gaussian 09W. Note the energy levels of HOMO and LUMO at S_1 state are different from that at the S_0 state. CT stands for conformation transformation. Excitation and radiative processes are marked as solid lines and the nonradiative processes are marked by dotted lines.

Similar to the result of probe **BS-2**, two absorption bands at 392 and 489 nm were found for **BS-2-OH**, which are close to

dx.doi.org/10.1021/jo202215x | J. Org. Chem. 2012, 77, 2192−2206

the experimental results (395 and 522 nm, Figure 7). The transitions are localized on the thienyl-BODIPY framework, the *p*-hydroxylphenyl moiety at the 8-position of the BODIPY core does not contribute to the transitions. This result is in agreement with the reported results of BODIPY dyes.[6a,c,28]

Furthermore, the emission of fluorophore was also studied, based on the optimized S_1 excited-state geometry (Table 3 and Figure 11). In stark contrast to the probe **BS-2**, the S_1 excited state of fluorophore **BS-2-OH** is probably an emissive excited state ($S_1 \rightarrow S_0$, $f = 0.6154$). The calculated emission is at 620 nm, which is close to the experimental results of 602 nm (Table 1, Figure 7). Thus, the fluorescence OFF-ON switching effect can be fully rationalized by the transformation from a dark S_1 excited state of the probe to the emissive S_1 excited state of the released free fluorophore, which is the result of cleavage of DNBS moiety by thiols, such as cysteine. To the best of our knowledge, the studies of fluorescence emission of a fluorophore with DFT calculations, based on the "electronic excited state", rather than "molecular orbitals", are rare. Herein the UV−vis absorption and the fluorescence emission are rationalized by a perspective of excited states, not molecular orbitals. Our result will inspire more investigations on the molecular probes by theoretical calculations. The in-depth understandings of the fluorescent probe from a perspective of theoretical chemistry will be useful for rational design of new fluorescence OFF−ON molecular probes with predetermined photophysical properties.

2.7. Thiol Probe with Thienyl Substitution at the 8-Position: Small Stokes Shift, Opposite Electron-Transfer Direction, and ON−OFF Fluorescence Transduction. In order to study the effect of substitution position of thienyl moiety on the photophysical properties of the thiol probe, fluorophore **BS-1-OH** was used to prepare a thiol probe **BS-1**. The UV−vis absorption of **BS-1** show maxima at 512 nm (Figure 12a). The probe **BS-1** shows an emission band at

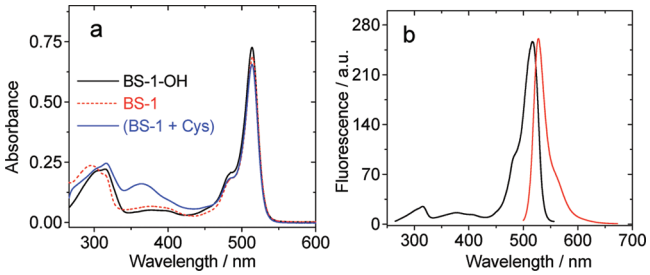

Figure 12. (a) UV−vis absorption spectra of probe **BS-1** (1.0×10^{-5} M) before and after treatment with Cys (200 equiv) for 20 min. The absorption of **BS-1-OH** is presented for comparison, 25 °C. (b) Emission and excitation spectra of probe **BS-1** (1.0×10^{-5} M). In mixed solution (DMF/H_2O = 4/1, v/v). λ_{ex} = 517 nm, 25 °C.

528 nm; thus, a small Stokes shift of 16 nm was observed, which is in stark contrast to the large Stokes shift of probe **BS-2**. These results imply that the 8-thienyl substitution is not involved in the frontier molecular orbitals of **BS-1**.[6a] This conclusion is supported by a similar thienyl-substituted BODIPY fluorophore, which shows similar emission wavelength and small Stokes shifts (<30 nm).[6g]

Interestingly, the fluorescence of **BS-1** was decreased in the presence of thiols, such as cysteine (Figure 13). This is in stark contrast to the fluorescence switch ON effect with probe **BS-2** in the presence of thiols (Figure 7).

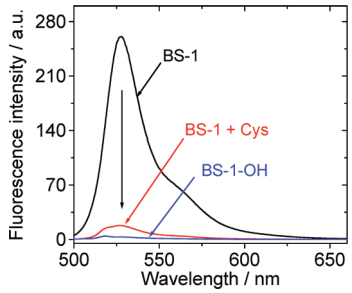

Figure 13. Fluorescence response of probe **BS-1** (1.0×10^{-5} M) before and after treatment with Cys (200 equiv) for 20 min. The emission of **BS-1-OH** is presented for comparison. In mixed solvent DMF/H_2O (4:1, v/v). λ_{ex} = 517 nm. 25 °C.

The 8-thienyl moiety is isolated from the π-conjugation core of the BODIPY core; thus, the thienyl moiety acts as an electron donor. As a result, the normal photoinduced electron transfer (PET) in the DNBS-protected fluorophore type of thiol probe, i.e., with the fluorophore as the electron donor, is interrupted by the thienyl moiety. The frustrated PET may be responsible for the abnormal fluorescence transductions of probe **BS-1** and fluorophore **BS-1-OH**, that is, the fluorescence ON feature of the probe and the fluorescence OFF character of the free fluorophore. In toluene solution, the free fluorophore **BS-1-OH** gives smaller fluorescence quantum yield than the BODIPY derivatives with thienyl moieties at the 2- and 6-positions, such as **BS-SS** and **BS-DS**, etc. (Table 1). These features are opposite to the normal properties of the DNBS thiol probe; i.e., the probe is usually nonfluorescent but the free fluorophore is fluorescent.[15a,b,d,29]

Probe **BS-1** shows faster recognition kinetics than probe **BS-2** (Figure 14). The selectivity of the probe toward different thiols and other biologically related analytes, such as glycine, etc., was also studied (Figure 14b). Good selectivity was found for the probe toward thiols over other biologically related molecules.

In order to rationalize the emission property of probe **BS-1** and the fluorophore **BS-1-OH**, the UV−vis absorption and the fluorescence emission were studied with DFT calculations (Figure 15 and Table 1). The S_1 state of **BS-1-OH** is a dark state, which means that the direct photoexcitation into S_1 state ($S_0 \rightarrow S_1$ transition) and radiative $S_1 \rightarrow S_0$ transition are forbidden, thus this fluorophore is most probably nonfluorescent. The calculated UV−vis absorption band of **BS-1-OH** is located at 419 nm.

By examination of the molecular orbitals involved in the S_1 excited state, it is clear that the thienyl moiety is an electron *donor* for PET (Figure 15). Thus the lack of fluorescence of fluorophore **BS-1-OH** is due to the photoinduced electron transfer from the thienyl moiety to the BODIPY chromophore.

The UV−vis absorption and emission of probe **BS-1** were also studied with the TDDFT methods (Figure 16 and Table 4). The calculated UV−vis absorption are close to the experimental results. For the emission, we observed a dark excited state (S_1 state) (f = 0.0000). However, the radiative decay from S_6 state is possible, and it is probably responsible for the emission of the probe at 528 nm (Figure 16).

2.8. Conclusion. In conclusion, new BODIPY fluorophores with thienyl substituents at the 2- or 2,6-position of BODIPY core (via C−C single bond connection) that show large Stokes shifts (96 nm) were prepared by a de novo approach, that is, by increasing the *geometry relaxation* of the fluorophore upon

dx.doi.org/10.1021/jo202215x | J. Org. Chem. 2012, 77, 2192−2206

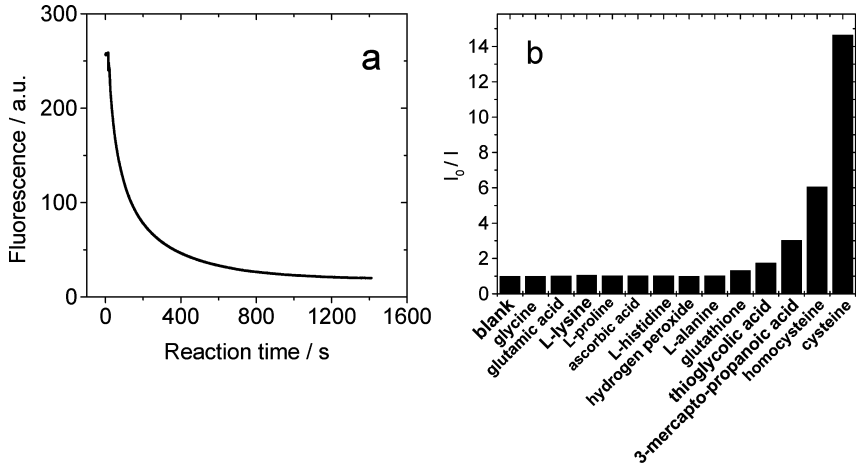

Figure 14. (a) Reaction kinetic curve of **BS-1** (1.0×10^{-5} M) with 200 equiv of **Cys**. (b) Fluorescence response of **BS-1** (1.0×10^{-5} M) to different analytes before and after incubation in the presence of 200 equiv of analytes for 180 min in DMF/water (4/1, v/v). λ_{ex} = 517 nm. λ_{em} = 526 nm. 37 °C.

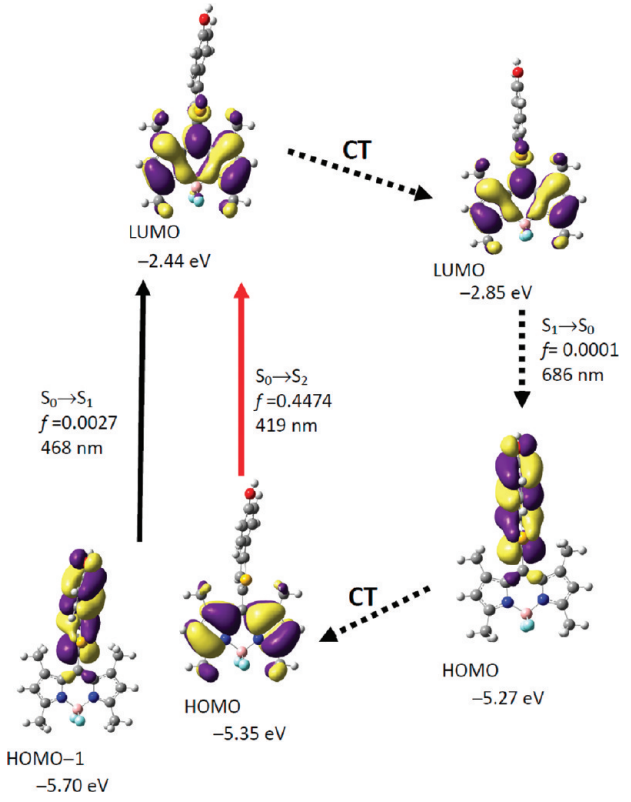

Figure 15. Rationalization of the UV−vis absorption and non-fluorescent feature of **BS-1-OH**: Frontier molecular orbitals (MOs) involved in the vertical excitation (i.e., UV−vis absorption, the left two columns) and emission (the right column) of **BS-1-OH**. Methanol was used as the solvent (PCM model). The vertical excitation related calculations are based on the optimized ground state geometry (S_0 state), the emission related calculations were based on the optimized excited state (S_1 state), at the B3LYP/6-31G(d) level using Gaussian 09W. Note the energy levels of HOMO and LUMO at S_1 state are different from that at S_0 state. CT stands for conformation transformation. Excitation and radiative processes are marked as solid lines and the nonradiative processes are marked by dotted lines. The lack of emission of **BS-1-OH** is due to the dark excited state (S_1).

photoexcitation. BODIPY with thienyl substitution at 2-position, **BS-SS**, shows strong absorption in the green range (ε = 69000 M^{-1} cm^{-1} at 513 nm), and red emission (λ_{em} = 591 nm, Φ_F = 20.6% in toluene). Control compounds with thienyl substituents at 8-position show the typical small Stokes shift (ca. 12 nm). DFT and TDDFT calculations proved that large geometry relaxation upon photoexcitation is responsible for the large Stokes shifts. Conversely, small geometry relaxation upon photoexcitation leads to small Stokes shifts.

The new BODIPY derivatives were used for design of thiol probes based on the 2,4-dinitrobenzenesulfonyl (DNBS) protection group (the fluorescence is modulated by the attachment or removal of DNBS moiety from the fluorophore). With different thienyl substitution profiles, fluorescence OFF−ON and ON−OFF responses were observed for the probes. For the probe with 2,6-dithienyl, thienyl moiety is involved in π-conjugation framework and thus the thienyl/BODIPY core acts as an integrated electron donor. As a result fluorescence OFF−ON switching was observed upon recognition of thiols such as cysteine. For the probe with 8-thienyl substitution, however, no π-conjugation between the thienyl and BODIPY core exists, thus the isolated thienyl acts as an electron donor. As a result, **BS-1** gives fluorescence ON−OFF response upon recognition of thiols, which is opposite to probe **BS-2**. To the best of our knowledge, this is the first time that a fluorescence ON-OFF DNBS-protected fluorophore thiol probe was reported, illustrating the elusive photophysics of the thiol probes that based on the DNBS protection strategy.

Our de novo approach to access large Stokes shift of BODIPY derivatives by increasing the geometry relaxation of the fluorophores upon photoexcitation, the design of the thiol probes, the fluorescence ON−OFF effect of the DNBS-based thiol probe, rationalization of the photophysical properties by DFT calculations, is useful for design of fluorophores that show large Stokes shift, as well as the related fluorescent molecular probes.

3. EXPERIMENTAL SECTION

3.1. Synthesis of 1. To the solution of 4-iodophenol (1.1 g, 5 mmol) in toluene (25 mL), ethanol (25 mL), 5-formylthiophene-2-boronic acid (1.56 g, 10 mmol) and $K_3PO_4 \cdot 3H_2O$ (2.67 g, 10 mmol) were added. $Pd(OAc)_2$ (58.4 mg, 0.6 mmol) was added under Ar. The mixture was refluxed at 80 °C for 8 h. After complete consumption of the starting material, the solution was evaporated under reduced pressure. The residual was purified by column chromatography (silica gel, CH_2Cl_2/CH_3OH = 100:1, v/v). A red solid was obtained, 410.0 mg,

dx.doi.org/10.1021/jo202215x | J. Org. Chem. 2012, 77, 2192−2206

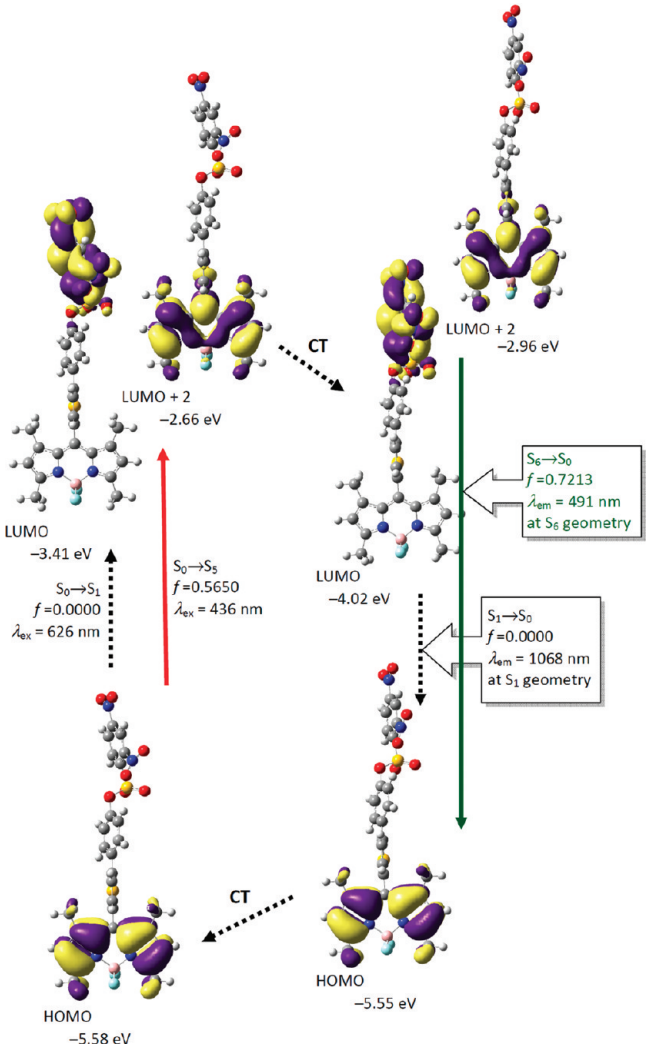

Figure 16. Rationalization of the UV−vis absorption, emission and the *small* Stokes shift of **BS-1**: frontier molecular orbitals (MOs) involved in the vertical excitation (i.e., UV−vis absorption, the left two columns) and emission (the right column) of **BS-1**. Methanol was used as solvent for DFT calculations. The vertical excitation related calculations are based on the optimized ground-state geometry (S_0 state), the emission related calculations were based on the optimized excited state (S_1 state), at the B3LYP/6-31G(d)/level using Gaussian 09W. CT stands for conformation transformation. Excitation and radiative processes are marked as solid lines, and the nonradiative processes are marked by dotted lines.

yield 40.2%. ^{1}H NMR (400 MHz, $CDCl_3$): δ 9.86 (s, 1H); 7.72(d, 1H, J = 3.8 Hz), 7.58 (d, 2H, J = 8.5 Hz), 7.30 (d, 1H, J = 4.0 Hz); 6.91(d, 2H, J = 8.4 Hz). ^{13}C NMR (100 MHz, $CDCl_3$): δ 183.3, 158.6, 155.7, 140.6, 138.6, 127.9, 127.1, 124.5, 122.7, 121.2, 116.0. TOF MS EI$^+$ ($C_{11}H_8O_2S$): calcd 204.0245, found 204.0252.

3.2. Synthesis of BS-1-OH. Compound **1** (400.0 mg, 1.86 mmol) was dissolved in THF (100 mL). 2,4-Dimethylpyrrole (0.72 mL, 5.9 mmol) and several drops of trifluoroacetic acid were added under Ar atmosphere. The reaction mixture was stirred at rt overnight, a solution of 2,3-dichloro-5,6-dicyano-*p*-benzoquinone (DDQ) (0.46 g, 1.96 mmol) in THF (100 mL) was added, and the mixture was stirred for 4 h. Triethylamine (TEA) (5.9 mL) and $BF_3{\cdot}OEt_2$ (5.9 mL) were consecutively added dropwise to the mixture cooled by an ice−water bath. The mixture was stirred overnight until thin-layer chromatography (TLC) (CH_2Cl_2/*n*-hexane =10/1, v/v) showed the reaction was completed. The solvent was removed under reduced pressure. The residue was dissolved in CH_2Cl_2, and the organic phase was washed with saturated $NaHCO_3$ (100 mL) and water (100 mL). The combined organic layers were dried over anhydrous Na_2SO_4, and the solvent was evaporated under reduced pressure. The crude product was purified by column chromatography (silica gel, CH_2Cl_2) to obtain a red powder (235.6 mg), yield 30.0%. Mp >250 °C. ^{1}H NMR (400 M Hz, $CDCl_3$): δ 7.52 (d, 2H, J = 8.6 Hz), 7.21 (d, 1H, J = 3.7 Hz); 6.91 (d, 1H, J = 3.7 Hz), 6.86 (d, 2H, J = 8.5 Hz), 6.01 (s, 2H), 4.98 (s, 1H), 2.56 (s, 6H), 1.73 (s, 6H); ^{13}C NMR (100 MHz, $CDCl_3$): δ 161.1, 159.9, 151.0, 147.6, 138.0, 136.4, 135.8, 132.7, 131.1, 129.2, 125.7, 125.4, 119.7, 18.3, 17.6. TOF HRMS ES$^+$ ($C_{23}H_{21}N_2BF_2OS$) calcd 422.1436, found 422.1440.

3.3. Synthesis of BS-1. To the solution of **BS-1-OH** (60.0 mg, 0.14 mmol) in a mixture of CH_2Cl_2 (5 mL) and TEA (0.1 mL) was added dropwise 2,4-dinitrobenzenesulfonyl chloride (DNBS, 112.0 mg, 0.42 mmol) in CH_2Cl_2 (5 mL). The mixture was stirred at rt for 4 h. When TLC showed that the reaction was completed, the reaction mixture was washed with water (3 × 20 mL) and the aqueous layers were extracted with CH_2Cl_2. The combined organic layers were dried over anhydrous Na_2SO_4 and evaporated under reduced pressure. The crude product was purified by column chromatography (silica gel, *n*-hexane/CH_2Cl_2 = 2/3, v/v) to give a red powder (45.6 mg), yield 50.0%. ^{1}H NMR (400 MHz, $CDCl_3$): δ 8.68 (d, 1H, J = 2.0 Hz), 8.53− 8.51 (m, 1H), 8.26 (d, 1H, J = 8.5 Hz), 7.64 (d, 2H, J = 8.8 Hz), 7.33 (d, 1H, J = 3.7 Hz), 7.27 (d, 2H, J = 8.8 Hz), 6.98 (d, 1H, J = 3.7 Hz), 6.02 (s, 2H), 2.56 (s, 6H), 1.70 (s, 6H). Mp 130.8 °C−132.4 °C. ^{13}C NMR (100 MHz, $CDCl_3$): δ 156.5, 144.3, 143.3, 135.1, 133.9, 133.7, 129.2, 127.4, 126.4, 124.3, 122.7, 121.7, 120.4, 14.7, 13.9. TOF LD$^+$ ($C_{29}H_{23}BN_4F_2S_2O_7$) calcd 652.1069, found 652.1130.

3.4. Synthesis of 2. The synthesis procedure is similar to that of **BS-1-OH**. The crude product was purified by column chromatography (silica gel, CH_2Cl_2) to obtain a red solid powder (1.22 g), yield 40.0%. ^{1}H NMR (400 M Hz, $CDCl_3$): δ 7.14 (d, 2H, J = 8.5 Hz), 6.96 (d, 2H, J = 8.5 Hz), 5.98 (s, 2H), 5.04 (s, 1H), 2.55 (s, 6H), 1.44 (s, 6H). ^{13}C NMR (100 MHz, $CDCl_3$ and CD_3OD): δ 157.6, 155.0, 143.4, 142.5, 131.9, 129.1, 125.8, 121.1, 116.1, 46.7, 14.5. TOF HRMS ES$^+$ ($C_{19}H_{19}BN_2OF_2$): calcd 340.1559, found 340.1570.

3.5. Synthesis of 3. Compound **2** (200.0 mg, 0.58 mmol) was dissolved CH_2Cl_2 (10 mL). *N*,*N*-Diisopropylethylamine (*i*-Pr_2NEt) (1.28 mmol, 0.21 mL) and chloromethyl ether (MOMCl, 0.87 mmol, 65.2 μL) were added. The reaction mixture was stirred at 60 °C for 6 h. When TLC (*n*-hexane/CH_2Cl_2 = 1/2 as eluent) showed that the reaction was complete, a saturated NH_4Cl solution (10 mL) was added in an ice−water bath and the mixture was stirred for 10 min. The solution was extracted with CH_2Cl_2 and dried over anhydrous Na_2SO_4. The solvent was evaporated under reduced pressure. The crude product was purified by column chromatography (silica gel, *n*-hexane/CH_2Cl_2 = 1/2, v/v) to give red powder (111.4 mg), yield 50.0%. ^{1}H NMR (400 M Hz, $CDCl_3$): δ 7.19−7.13 (m, 4H); 5.98 (s, 2H); 5.23 (s, 2H); 3.52 (s, 3H); 2.55 (s, 6H); 1.43 (s, 6H). ^{13}C NMR (100 MHz, $CDCl_3$): δ 157.9, 155.3, 143.1, 141.7, 131.8, 129.2, 128.3, 121.1, 116.8, 94.6, 56.2, 29.7, 14.5. TOF HRMS ES$^+$ ($C_{21}H_{23}BN_2O_2F_2$): calcd 384.1821, found 384.1827.

3.6. Synthesis of 4. To the solution of compound **3** (100.0 mg, 0.26 mmol) in CH_2Cl_2(10 mL) was added *N*-iodosuccinimide (NIS) (572.4 mg, 2.54 mmol), and the mixture was stirred for 2 h. After completely consumption of **3**, the solvent was evaporated under reduced pressure. The residual was purified by column chromatography (silica gel, *n*-hexane/CH_2Cl_2 = 1/1, v/v) to give a red solid (132.3 mg), yield 80.0%. ^{1}H NMR (400 MHz, $CDCl_3$): δ 7.19 (m, 4H); 5.25 (s, 2H); 3.53 (s, 2H); 2.64 (s, 6H); 1.45 (s, 6H). ^{13}C NMR (100 MHz, $CDCl_3$): δ 158.3, 156.7, 145.4, 141.4, 131.6, 129.1, 127.9, 117.1, 94.6, 56.2, 29.7, 17.2, 16.0. TOF HRMS ES$^+$ ($C_{21}H_{21}N_2O_2BF_2I_2$): calcd 635.9754, found 635.9757.

3.7. Synthesis of 5. The synthesis procedure is similar to that of **1**. The crude product was purified by column chromatography (silica gel, *n*-hexane/CH_2Cl_2 = 2/1, v/v) to give a red solid (58.8 mg), yield 67.0%. ^{1}H NMR (400 MHz, $CDCl_3$): δ 7.35 (d, 2H, J = 5.2 Hz), 7.24 (d, 2H, J = 8.6 Hz), 7.17 (d, 2H, J = 5.8 Hz), 7.09 (t, 2H, J = 3.5 Hz), 6.86 (d, 2H, J = 3.5 Hz), 5.23 (s, 2H), 3.50 (s, 2H), 2.60 (s, 6H), 1.44 (s, 6H). ^{13}C NMR (100 MHz, $CDCl_3$): δ 158.1, 155.1, 142.5, 140.8,

dx.doi.org/10.1021/jo202215x | *J. Org. Chem.* 2012, 77, 2192−2206

Table 4. Selected Parameters for the Vertical Excitation (UV−vis Absorptions) and the Emission of the BODIPY Derivatives: Electronic Excitation Energies (eV) and Oscillator Strengths (f), Configurations of the Low-Lying Excited States of the Compounds; Calculation of the S_0/S_1 Energy Gaps Based on the Optimized Ground-State Geometries (UV−vis Absorption) and the Optimized Excited-State Geometries (Fluorescence) (Methanol Was Used as Solvent, Calculated at TDDFT//B3LYP/6-31G(d) Level with Gaussian 09W)

			TDDFT//B3LYP/6-31G(d)			
compound		electronic transitions[a]	excitation energy	f[b]	composition[c]	CI[d]
BS-1-OH	absorption[e]	$S_0 \rightarrow S_1$	2.43 eV (511 nm)	0.0032	H-1→L	0.6930
		$S_0 \rightarrow S_2$	2.85 eV (436 nm)	0.5686	H-2→L	0.1240
					H→L	0.6943
BS-1-OH	emission[f]	$S_1 \rightarrow S_0$	1.81 eV (686 nm)	0.0001	H→L	0.7021
		$S_2 \rightarrow S_0$	2.59 eV (478 nm)	0.7776	H-1→L	0.7055
		$S_3 \rightarrow S_0$	3.03 eV (409 nm)	0.0290	H-2→L	0.7014
		$S_4 \rightarrow S_0$	3.29 eV (376 nm)	0.0136	H-3→L	0.7020
		$S_5 \rightarrow S_0$	3.45 eV (359 nm)	1.1380	H→L+1	0.6964
		$S_6 \rightarrow S_0$	3.57 eV (347 nm)	0.0005	H-6→L	0.3135
					H-4→L	0.6317
BS-1	absorption[e]	$S_0 \rightarrow S_1$	1.98 eV (626 nm)	0.0000	H→L	0.7068
		$S_0 \rightarrow S_5$	2.84 eV (436 nm)	0.5650	H-2→L+2	0.1250
					H→L+2	0.6997
		$S_0 \rightarrow S_6$	2.31 eV (535 nm)	0.0000	H-3→L	0.7069
BS-1	emission	$S_1 \rightarrow S_0$[f]	1.16 eV (1068 nm)	0.0001	H→L	0.7070
		$S_6 \rightarrow S_0$[g]	2.53 eV (491 nm)	0.7213	H→L+2	0.7018

[a]Only selected excited states were considered. The numbers in parentheses are the excitation energy in wavelength. [b]Oscillator strength. [c]H stands for HOMO and L stands for LUMO. Only the main configurations are presented. [d]Coefficient of the wave function for each excitations. The CI coefficients are in absolute values. [e]The calculations on UV−vis absorption are based on the optimized ground-state geometry. [f]The calculations on fluorescence are based on the optimized S_1 state geometry. [g]The calculations on fluorescence are based on the optimized S_6 state geometry.

134.3, 131.6, 129.3, 128.3, 127.7, 127.2, 126.0, 171.0, 94.6, 56.2, 29.7, 13.5, 13.1. TOF HRMS ES$^+$ ($C_{29}H_{27}N_2O_2F_2S_2B$): calcd 548.1575, found 548.1577.

3.8. Synthesis of BS-2-OH. To the solution of **5** (77.1 mg, 0.14 mmol) in ethanol (10 mL) was added 6 mol/L of hydrochloric acid (42 μL, 0.25 mmol) in an ice−water bath, and the mixture was stirred at 60 °C for 4 h. The solvent was evaporated under reduced pressure. The residue was washed with water (3 × 20 mL), followed by extraction with CH_2Cl_2. The organic layers were dried over anhydrous Na_2SO_4 and evaporated under reduced pressure. The crude product was purified by column chromatography (silica gel, *n*-hexane/CH_2Cl_2 = 1/1, v/v) to give a red powder (40.0 mg), yield 56.7%. mp >250 °C. ^{1}H NMR (400 MHz, $CDCl_3$): δ 7.36 (d, 2H, J = 5.5 Hz), 7.20 (d, 2H, J = 8.3 Hz), 7.10 (t, 2H, 4.0 Hz), 6.99 (d, 2H, J = 7.5 Hz), 6.86 (s, 2H), 2.60 (s, 6H), 1.45 (s, 6H). ^{13}C NMR (100 MHz, $CDCl_3$): δ 151.9, 149.1, 146.4, 140.7, 126.9, 124.7, 123.4, 91.9, 29.3, 26.8, 26.6, 20.2, 11.6. TOF HRMS ES$^+$ ($C_{27}H_{23}N_2OS_2BF_2$): calcd 504.1313, found 504.1323.

3.9. Synthesis of BS-2. To the solution of **BS-2-OH** (35.0 mg, 0.10 mmol) in CH_2Cl_2 (5 mL) and TEA (0.1 mL) was added dropwise a solution of 2,4-dinitrobenzenesulfonyl chloride (DNBS. 60.0 mg, 0.3 mmol) in CH_2Cl_2 (5 mL), and the mixture was stirred at rt for 3 h. When TLC showed complete consumption of the starting material, the solution was washed with water (3 × 20 mL), and the aqueous layers were extracted with CH_2Cl_2. The combined organic layers were dried over anhydrous Na_2SO_4 and evaporated under reduced pressure. The crude product was purified by column chromatography (silica gel, *n*-hexane/CH_2Cl_2 = 3/2, v/v) to give a red powder (25.0 mg), yield 34.0%. Mp: 96.3−99.5 °C. ^{1}H NMR (400 MHz, $CDCl_3$): δ 8.67 (s, 1H), 8.47 (d, 1H, J = 8.7 Hz), 8.18 (d, 2H, J = 8.5 Hz), 7.41 (s, 4H), 7.38 (d, 2H, J = 4.1 Hz), 7.11 (t, 2H, J = 3.7 Hz), 6.86 (d, 2H, J = 2.6 Hz), 2.59 (s, 6H), 1.34 (s, 6H). ^{13}C NMR (100 MHz, $CDCl_3$): δ 156.2, 151.1, 149.6, 149.4, 140.1, 135.5, 133.8, 133.8, 133.4, 131.0, 130.4, 128.0, 127.4, 127.0, 126.3, 123.3, 120.5, 41.9, 31.6, 29.7, 22.7, 13.6, 13.2. TOF MS ES$^+$ ($C_{33}H_{24}BN_4O_7F_2S_3Na^+$) calcd 757.0844, found 757.0531. TOF LD$^-$ ($C_{33}H_{23}BN_4O_7F_2S_3^+$): calcd 733.0868, found 733.0892.

3.10. Synthesis of 6. Benzoyl chloride (1.4 g, 11 mmol) was dissolved in CH_2Cl_2 (150 mL), and 2,4-dimethylpyrrole (2.0 mL, 20 mmol) was added under Ar atmosphere. After the reaction mixture was stirred at rt overnight, triethylamine (TEA) (10 mL) and $BF_3{\cdot}OEt_2$ (10 mL) were added dropwise in an ice−water bath, and the mixture was stirred overnight until thin-layer chromatography (TLC) (CH_2Cl_2) showed that the reaction was completed. The solvent was removed under reduced pressure to obtain a residue which was dissolved in CH_2Cl_2 and washed with saturated Na_2CO_3 (100 mL) and water (100 mL). The combined organic layers were dried over anhydrous Na_2SO_4 and evaporated under reduced pressure. The crude product was purified by column chromatography (silica gel, CH_2Cl_2) to obtain a red powder (1.96 g), yield 55.0%. ^{1}H NMR (400 MHz, $CDCl_3$): δ 7.49−7.47 (m, 3H), 7.29−7.26 (m, 2H), 5.98 (s, 2H), 2.56 (s, 6H), 1.37 (s, 6H).

3.11. Synthesis of 7. To the solution of **6** (200.0 mg, 0.62 mmol) in CH_2Cl_2 (50 mL) was added dropwise *N*-iodosuccinimide (NIS) (140.0 mg, 0.62 mmol) in CH_2Cl_2 (20 mL), and the mixture was stirred for 1 h. After complete consumption of **6**, the reaction mixture was evaporated under reduced pressure. The residual was purified by column chromatography (silica gel, *n*-hexane/CH_2Cl_2 = 2/1, v/v) to give a bright red solid (125.6 mg), yield 45.0%. ^{1}H NMR (400 MHz, $CDCl_3$): δ 7.51−7.48 (m, 3H), 7.27−7.25 (m, 2H), 6.04 (s, 1H), 2.63 (s, 3H), 2.57 (s, 3H), 1.38 (s, 6H). TOF LD$^+$ ($[C_{19}H_{18}BF_2IN_2]^+$): calcd 450.0576, found 450.0535.

3.12. Synthesis of 8. The synthesis procedure is similar to that of **4**. The crude product was purified by column chromatography (silica gel, *n*-hexane/CH_2Cl_2 = 1/1, v/v). Red solid was obtained (137.5 mg), yield 77.0%. ^{1}H NMR (400 MHz, $CDCl_3$): δ 7.54−7.51 (m, 3H), 7.26−7.24 (m, 2H), 2.65 (s, 6H), 1.38 (s, 6H). TOF LD$^-$ ($[C_{19}H_{17}BF_2I_2N_2]^-$): calcd 575.9542, found 575.9528.

3.13. Synthesis of BS-SS. The synthesis procedure is similar to that of **1**. The crude product was purified by column chromatography (silica gel, *n*-hexane/CH_2Cl_2 = 1/1, v/v) to give a red solid (56.6 mg), yield 63.4%. Mp: 155.2−157.2 °C. ^{1}H NMR (400 MHz, $CDCl_3$): δ 7.50 (d, 3H, J = 5.9 Hz); 7.33−7.30 (m, 3H); 7.08 (t, 1H, J = 3.6 Hz); 6.84 (d, 1H, J = 3.40 Hz); 6.02 (s, 1H), 2.58 (s, 6H), 1.39 (d, 2H, J = 11.0 Hz). ^{13}C NMR (100 MHz, $CDCl_3$): δ 156.7, 154.3, 144.1,

dx.doi.org/10.1021/jo202215x | J. Org. Chem. 2012, 77, 2192−2206

142.3, 140.3, 135.2, 134.7, 132.1, 130.9, 129.4, 129.2, 128.1, 127.8, 127.3, 126.0, 121.9, 30.5, 14.9, 14.7, 13.5, 12.9. TOF HRMS ES$^+$ ($C_{23}H_{21}BF_2N_2S$): calcd 406.1487, found 406.1498.

3.14. Synthesis of BS-DS. The synthesis procedure is similar to that of **1**. The crude product was purified by column chromatography (silica gel, *n*-hexane/CH_2Cl_2 = 1/1, v/v) to obtain a red solid (45.1 mg), yield 54.4%. Mp: >250 °C. ^{1}H NMR (400 MHz, $CDCl_3$): δ 7.51 (d, 3H, J = 6.6 Hz), 7.35−7.33 (m, 4H), 7.09 (t, 2H, J = 3.7 Hz), 6.86 (d, 2H, J = 3.5 Hz), 2.60 (s, 6H), 1.38 (s, 6H). ^{13}C NMR (100 MHz, $CDCl_3$): δ 155.5, 141.0, 129.5, 128.2, 127.9, 127.4, 126.2, 29.9, 13.7, 13.1. TOF HRMS ES$^+$ ($C_{27}H_{23}BN_2F_2S_2$): calcd 488.1364, found 488.1385.

3.15. Fluorescent Imaging of the Intracellular Thiols. The photographs were obtained using a Nikon ECLIPSE-Ti confocal laser scanning microscopy. The Hela cells were incubated with probes **BS-2** in PBS (phosphate buffered solution, pH 7.4) for 45 min at 37 °C, and red emission was observed with 543 nm laser excitation. In the control experiments, cells were incubated in the presence of 0.5 mM *N*-methylmaleimide in DMSO−PBS solution (1:200, v/v) for 1 h to remove the intracellular thiols. Then the cells were washed with PBS buffer for three times, and the probe (20 μM, 0.4: 200 DMSO/PBS, v/v, pH 7.4) was added and incubated at 37 °C for 45 min. Fluorescence imaging was taken after the cells were washed with PBS buffer for three times.

3.16. DFT Calculations. The ground-state structures of BODIPY derivatives and the thiol probes were optimized using DFT with B3LYP functional and 6-31G (d) basis set. The initial geometries of the compounds were generated by the GaussView software. The excited-state related calculations (UV−vis absorptions) were carried out with the time-dependent DFT (TDDFT) with the optimized structure of the ground state (DFT/6-31G(d)). The emission of the fluorophores were calculated based on the optimized S_1 excited state geometry, optimized by the TDDFT method. In some cases, higher excited states were optimized. There are no imaginary frequencies in frequency analysis of all calculated structures. All of these calculations were performed with Gaussian 09W.[30]

■ ASSOCIATED CONTENT

Supporting Information

Synthesis and structural characterization data of the fluorophores and the probes; solvent-dependent fluorescence spectra and DFT calculation information. This material is available free of charge via the Internet at http://pubs.acs.org.

■ AUTHOR INFORMATION

Corresponding Author

*E-mail: zhaojzh@dlut.edu.cn. Group homepage: http://finechem.dlut.edu.cn/photochem.

Notes

The authors declare no competing financial interest.

■ ACKNOWLEDGMENTS

We thank the NSFC (20972024 and 21073028), the Royal Society (UK) and NSFC (China−UK Cost-Share Science Networks, 21011130154), the Fundamental Research Funds for the Central Universities (DUT10ZD212 and DUT11LK19), the State Key laboratory of Fine Chemicals (KF0802 and KF0901), Ministry of Education (SRFDP-200801410004 and NCET-08-0077), and Dalian University of Technology for financial support.

■ REFERENCES

(1) (a) Kim, H.; Burghart, A.; Welch, M. B.; Reibenspies, J.; Burgess, K. *Chem. Commun.* **1999**, 1889−1890. (b) Rurack, K.; Kollmannsberger, M.; Daub, J. *Angew. Chem., Int. Ed.* **2001**, *40*, 385−387. (c) Wan, C. W.; Burghart, A.; Chen, J.; Bergstrom, F.; Johansson, L. B. A.; Wolford, M. F.; Kim, T. G.; Topp, M. R.; Hochstrasser, R. M.; Burgess, K. *Chem.—Eur. J.* **2003**, *9*, 4430−4441. (d) Azov, V. A.; Schlegel, A.; Diederich, F. *Angew. Chem., Int. Ed.* **2005**, *44*, 4635−4638. (e) Ulrich, G.; Nastasi, F.; Retailleau, P.; Puntoriero, F.; Ziessel, R.; Campagna, S. *Chem.—Eur. J.* **2008**, *14*, 4381−4392. (f) Zhu, M.; Jiang, L.; Yuan, M.; Liu, X.; Yang, C.; Zheng, H.; Yin, X.; Zuo, Z.; Liu, H.; Li, Y. *J. Polym. Sci.: Part A: Polym. Chem.* **2008**, *46*, 7401−7410. (g) Rachford, A. A.; Ziessel, R.; Bura, T.; Retailleau, P.; Castellano, F. N. *Org. Lett.* **2008**, *10*, 1581−1584. (h) Nastasi, F.; Puntoriero, F.; Campagna, S.; Diring, S.; Ziessel, R. *Phys. Chem. Chem. Phys.* **2008**, *10*, 3982−3986. (i) Belman, N.; Israelachvili, J. N.; Li, Y.; Safinya, C. R.; Bernstein, J.; Golan, Y. *J. Am. Chem. Soc.* **2009**, *131*, 9007−9013. (j) Descalzo, A. B.; Xu, H; Xue, Z.; Hoffmann, K.; Shen, Z.; Weller, M. G.; You, X.; Rurack, K. *Inorg. Chem.* **2010**, *49*, 3730−3736. (k) Kaloudi-Chantzea, A.; Karakostas, N.; Raptopoulou, C. P.; Psycharis, V.; Saridakis, E.; Griebel, J.; Hermann, R.; Pistolis, G. *J. Am. Chem. Soc.* **2010**, *132*, 16327−16329. (l) Kowada, T.; Yamaguchi, S.; Ohe, K. *Org. Lett.* **2010**, *12*, 296−299. (m) Nastasi, F.; Puntoriero, F.; Campagna, S.; Olivierb, J. H.; Ziessel, R. *Phys. Chem. Chem. Phys.* **2010**, *12*, 7392−7402. (n) Liu, J. Y.; El-Khouly, M. E.; Fukuzumi, S.; Ng, D. K. P. *Chem.—Eur. J.* **2011**, *17*, 1605−1613. (o) Gresser, R.; Hummert, M.; Hartmann, H.; Leo, K.; Riede, M. *Chem.—Eur. J.* **2011**, *17*, 2939−2947.

(2) (a) Gabe, Y.; Urano, Y.; Kikuchi, K.; Kojima, H.; Nagano, T. *J. Am. Chem. Soc.* **2004**, *126*, 3357−3367. (b) Wu, Y.; Peng, X.; Guo, B.; Fan, J.; Zhang, Z.; Wang, J.; Cui, A.; Gao, Y. *Org. Biomol. Chem.* **2005**, *3*, 1387−1392. (c) Baruah, M.; Qin, W.; Basarić, N.; Borggraeve, W. M. D.; Boens, N. *J. Org. Chem.* **2005**, *70*, 4152−4157. (d) Baruah, M.; Qin, W.; Vallée, R. A. L.; Beljonne, D.; Rohand, T.; Dehaen, W.; Boens, N. *Org. Lett.* **2005**, *7*, 4377−4380. (e) Coskun, A.; Deniz, E.; Akkaya, E. U. *Org. Lett.* **2005**, *7*, 5187−5189. (f) Coskun, A.; Akkaya, E. U. *J. Am. Chem. Soc.* **2006**, *128*, 14474−14475. (g) Matsumoto, T.; Urano, Y.; Shoda, T.; Kojima, H.; Nagano, T. *Org. Lett.* **2007**, *9*, 3375−3377. (h) Cheng, T.; Xu, Y.; Zhang, S.; Zhu, W.; Qian, X.; Duan, L. *J. Am. Chem. Soc.* **2008**, *130*, 16160−16161. (i) Ojida, A.; Sakamoto, T.; Inoue, M.; Fujishima, S.; Lippens, G.; Hamachi, I. *J. Am. Chem. Soc.* **2009**, *131*, 6543−6548. (j) Dodani, S. C.; He, Q.; Chang, C. J. *J. Am. Chem. Soc.* **2009**, *131*, 18020−18021. (k) Gómez-Durán, C. F. A.; García-Moreno, I.; Costela, A.; Martin, V.; Sastre, R.; Bañuelos, J.; Arbeloa, F. L.; Arbeloa, I. L.; Peña-Cabrera, E. *Chem. Commun.* **2010**, *46*, 5103−5105. (l) Li, X.; Qian, S.; He, Q.; Yang, B.; Li, J.; Hu, Y. *Org. Biomol. Chem.* **2010**, *8*, 3627−3630. (m) Sun, H.; Liu, S.; Ma, T.; Song, N.; Zhao, Q.; Huang, Wei. *New J. Chem.* **2011**, *35*, 1194−1197. (n) Cheng, T.; Wang, T.; Zhu, W.; Chen, X.; Yang, Y.; Xu, Y.; Qian, X. *Org. Lett.* **2011**, *13*, 3656−3659.

(3) (a) Zhang, X.; Xiao, Y.; Qian, X. *Org. Lett.* **2008**, *10*, 29−32. (b) Costela, A.; García-Moreno, I.; Pintado-Sierra, M.; Amat-Guerri, F.; Sastre, R.; Liras, M.; Arbeloa, F. L.; Prieto, J. B.; Arbeloa, I. L. *J. Phys. Chem. A* **2009**, *113*, 8118−8124. (c) Ueno, Y.; Jose, J.; Loudet, A.; Pérez-Bolívar, C. Jr.; Burgess., P. A. *J. Am. Chem. Soc.* **2011**, *133*, 51−55. (d) Lazarides, T.; McCormick, T. M.; Wilson, K. C.; Lee, S.; McCamant, D. W.; Eisenberg, R. *J. Am. Chem. Soc.* **2011**, *133*, 350−364.

(4) (a) Gorman, A.; Killoran, J.; O'Shea, C.; Kenna, T.; Gallagher, W. M.; O'Shea, D. F. *J. Am. Chem. Soc.* **2004**, *126*, 10619−10631. (b) Yogo, T.; Urano, Y.; Ishitsuka, Y.; Maniwa, F.; Nagano, T. *J. Am. Chem. Soc.* **2005**, *127*, 12162−12163. (c) Yogo, T.; Urano, Y.; Mizushima, A.; Sunahara, H.; Inoue, T.; Hirose, K.; Iino, M.; Kikuchi, K.; Nagano, T. *Proc. Natl. Acad. Sci. U.S.A.* **2008**, *105*, 28−32. (d) Adarsh, N.; Avirah, R. R.; Ramaiah, D. *Org. Lett.* **2010**, *12*, 5720−5723. (e) Awuah, S. G.; Polreis, J.; Biradar, V.; You, Y. *Org. Lett.* **2011**, *13*, 3884−3887.

(5) (a) Singh-Rachford, T. N.; Haefele, A.; Ziessel, R; Castellano, F. N. *J. Am. Chem. Soc.* **2008**, *130*, 16164−16165. (b) Singh-Rachford, T. N.; Castellano, F. N. *Coord. Chem. Rev.* **2010**, *254*, 2560−2573. (c) Wu, W.; Guo, H.; Wu, W.; Ji, S.; Zhao, J. *J. Org. Chem.* **2011**, *76*, 7056−7064. (d) Zhao, J.; Ji, S.; Guo, H. *RSC Adv.* **2011**, *1*, 937−950. (e) Ji, S.; Wu, W.; Wu, W.; Guo, H.; Zhao, J. *Angew. Chem., Int. Ed.* **2011**, *50*, 1626−1629. (f) Ji, S.; Guo, H.; Wu, W.; Wu, W.; Zhao, J. *Angew. Chem., Int. Ed.* **2011**, *50*, 8283−8286.

(6) (a) Ulrich, G.; Ziessel, R.; Harriman, A. *Angew. Chem., Int. Ed.* **2008**, *47*, 1184−1201. (b) Benniston, A. C.; Copley, G. *Phys. Chem. Chem. Phys.* **2009**, *11*, 4124−4131. (c) Ziessel, R.; Harriman, A. *Chem. Commun.* **2011**, *47*, 611−631. (d) Loudet, A.; Burgess, K. *Chem. Rev.* **2007**, *107*, 4891−4932. (e) Peña-Cabrera, E.; Aguilar-Aguilar, A.; González-Domínguez, M.; Lager, E.; Zamudio-Vázquez, R.; Godoy-Vargas, J.; Villanueva-García, F. *Org. Lett.* **2007**, *9*, 3985−3988. (f) Kim, K.; Jo, C.; Easwaramoorthi, S.; Sung, J.; Kim, D. H.; Churchill, D. G. *Inorg. Chem.* **2010**, *49*, 4881−4894. (g) Choi, S. H.; Kim, K.; Lee, J.; Do, Y.; Churchill, D. G. *J. Chem. Crystallogr.* **2007**, *37*, 315−331.

(7) (a) Ulrich, G.; Ziessel, R. *J. Org. Chem.* **2004**, *69*, 2070−2083. (b) Rohand, T.; Baruah, M.; Qin, W.; Boens, N.; Dehaen, W. *Chem. Commun.* **2006**, 266−268. (c) Jiao, L.; Yu, C.; Li, J.; Wang, Z.; Wu, M.; Hao, E. *J. Org. Chem.* **2009**, *74*, 7525−7528. (d) Palma, A.; Tasior, M.; Frimannsson, D. O.; Vu, T. T.; Meallet-Renault, R.; O'Shea, D. F. *Org. Lett.* **2009**, *11*, 3638−3641. (e) Mula, S.; Ulrich, G.; Ziessel, R. *Tetrahedron Lett.* **2009**, *50*, 6383−6388. (f) Zhu, S.; Zhang, J.; Vegesna, G. K.; Pandey, R.; Luo, F. T.; Greena, S. A.; Liu, H. *Chem. Commun.* **2011**, *47*, 3508−3510. (g) Zhu, S.; Zhang, J.; Vegesna, G.; Luo, F. T.; Green, S. A.; Liu, H. *Org. Lett.* **2011**, *13*, 438−441.

(8) Lee, J. S.; Kang, N.; Kim, Y. K.; Samanta, A.; Feng, S.; Kim, H. K.; Vendrell, M.; Park, J. H.; Chang, Y. T. *J. Am. Chem. Soc.* **2009**, *131*, 10077−10082.

(9) Bellier, Q.; Pegaz, S.; Aronica, C.; Guennic, B. L.; Andraud, C.; Maury, O. *Org. Lett.* **2011**, *13*, 22−25.

(10) (a) Lakowicz, J. R. *Principles of Fluorescence Spectroscopy*, 2nd ed.; Kluwer Academic: New York, 1999. (b) Valeur, B. *Molecular Fluorescence: Principles and Applications*; Wiley-VCH Verlag: Weinheim, 2001.

(11) (a) Rurack, K.; Kollmannsberger, M.; Daub, J. *New J. Chem.* **2001**, *25*, 289−292. (b) Coskun, A.; Akkaya, E. U. *J. Am. Chem. Soc.* **2005**, *127*, 10464−10465. (c) Baruah, M.; Qin, W.; Flors, C.; Hofkens, J.; Vallée, R. A. L.; Beljonne, D.; Auweraer, M. V.; Borggraeve, W. M. D.; Boens, N. *J. Phys. Chem. A* **2006**, *110*, 5998−6009. (d) Fron, E.; Coutiño-Gonzalez, E.; Pandey, L.; Sliwa, M.; Auweraer, M. V.; Schryver, F. C. D.; Thomas, J.; Dong, Z.; Leen, V.; Smet, M.; Dehaen, W.; Vosch, T. *New J. Chem.* **2009**, *33*, 1490−1496. (e) Rihn, S.; Retailleau, P.; Bugsaliewicz, N.; Nicola, A. D.; Ziessel, R. *Tetrahedron Lett.* **2009**, *50*, 7008−7013. (f) Ziessel, R.; Rihn, S.; Harriman, A. *Chem.—Eur. J.* **2010**, *16*, 11942−11953. (g) Filatov, M. A.; Lebedev, A. Y.; Mukhin, S. N.; Vinogradov, S. A.; Cheprakov, A. V. *J. Am. Chem. Soc.* **2010**, *132*, 9552−9554. (h) Jiao, L.; Yu, C.; Liu, M.; Wu, Y.; Cong, K.; Meng, T.; Wang, Y.; Hao, E. *J. Org. Chem.* **2010**, *75*, 6035−6038. (i) Jiao, L.; Yu, C.; Uppal, T.; Liu, M.; Li, Y.; Zhou, Y.; Hao, E.; Hu, X.; Vicente, M. G. H. *Org. Biomol. Chem.* **2010**, *8*, 2517−2519. (j) Shao, J.; Guo, H.; Ji, S.; Zhao, J. *Biosen. Bioelectron.* **2011**, *26*, 3012−3017. (k) Bura, T.; Retailleau, P.; Ulrich, G.; Ziessel, R. *J. Org. Chem.* **2011**, *76*, 1109−1117.

(12) (a) Harriman, A.; Mallon, L. J.; Elliot, K. J.; Haefele, A.; Ulrich, G.; Ziessel, R. *J. Am. Chem. Soc.* **2009**, *131*, 13375−13386. (b) Ziessel, R.; Rihn, S.; Harriman, A. *Chem.—Eur. J.* **2010**, *16*, 8832−8845.

(13) Guliyev, R.; Coskun, A.; Akkaya, E. U. *J. Am. Chem. Soc.* **2009**, *131*, 9007−9013.

(14) Turro, N. J.; Ramamurthy, V.; Scaiano, J. C. *Principles of Molecular Photochemistry: An Introduction*; University Science Books: Sausalito, 2009.

(15) (a) Reisinger, A.; Trapp, N.; Krossing, I.; Altmannshofer, S.; Herz, V.; Presnitz, M.; Scherer, W. *Angew. Chem., Int. Ed.* **2007**, *46*, 8445−8448. (b) Bouffard, J.; Kim, Y.; Swager, T. M.; Weissleder, R.; Hilderbrand, S. A. *Org. Lett.* **2008**, *10*, 37−40. (c) Ji, S.; Yang, J.; Yang, Q.; Liu, S.; Chen, M.; Zhao, J. *J. Org. Chem.* **2009**, *74*, 4855−4865. (d) Wang, S.; Deng, W.; Sun, D.; Yan, M.; Zheng, H.; Xu, J. *Org. Biomol. Chem.* **2009**, *7*, 4017−4020. (e) Ji, S.; Guo, H.; Yuan, X.; Li, X.; Ding, H.; Gao, P.; Zhao, C.; Wu, W.; Wu, W.; Zhao, J. *Org. Lett.* **2010**, *12*, 2876−2879. (f) Guo, H.; Jing, Y.; Yuan, X.; Ji, S.; Zhao, J.; Li, X.; Kan, Y. *Org. Biomol. Chem.* **2011**, *9*, 3844−3853.

(16) (a) Goze, C.; Ulrich, G.; Mallon, L. J.; Allen, B. D.; Harriman, A.; Ziessel, R. *J. Am. Chem. Soc.* **2006**, *128*, 10231−10239. (b) Sunahara, H.; Urano, Y.; Kojima, H.; Nagano, T. *J. Am. Chem. Soc.* **2007**, *129*, 5597−5604. (c) Bozdemir, O. A.; Sozmen, F.; Buyukcakir, O.; Guliyev, R.; Cakmak, Y.; Akkaya, E. U. *Org. Lett.* **2010**, *12*, 1400−1403. (d) Haefele, A.; Zedde, C.; Retailleau, P.; Ulrich, G.; Ziessel, R. *Org. Lett.* **2010**, *12*, 1672−1675.

(17) Ulrich, G.; Goeb, S.; Nicola, A. D.; Retailleau, P.; Ziessel, R. *J. Org. Chem.* **2011**, *76*, 4489−4505.

(18) Gareis, T.; Huber, C.; Wolfbeis, O. S.; Daub, J. *Chem. Commun.* **1997**, 1717−1718.

(19) (a) Rohand, T.; Qin, W.; Boens, N.; Dehaen, W. *Eur. J. Org. Chem.* **2006**, 4658−4663. (b) Bonardi, L.; Ulrich, G.; Ziessel, R. *Org. Lett.* **2008**, *10*, 2183−2186. (c) Leen, V.; Braeken, E.; Luckermans, K.; Jackers, C.; Auweraer, M. V.; Boens, N.; Dehaen, W. *Chem. Commun.* **2009**, 4515−4517. (d) Zhang, D.; Wang, Y.; Xiao, Y.; Qian, S.; Qian, X. *Tetrahedron.* **2009**, *65*, 8099−8103. (e) Chase, D. T.; Young, B. S.; Haley, M. M. *J. Org. Chem.* **2011**, *76*, 4043−4051.

(20) Algia, F.; Cihaner, A. *Org. Electron.* **2009**, *10*, 453−458.

(21) Ning, Z.; Tian, H. *Chem. Commun.* **2009**, 5483−5495.

(22) (a) Kee, H. L.; Kirmaier, C.; Yu, L.; Thamyongkit, P.; Youngblood, W. J.; Calder, M. E.; Ramos, L.; Noll, B. C.; Bocian, D. F.; Scheidt, W. R.; Birge, R. R.; Lindsey, J. S.; Holten, D. *J. Phys. Chem. B.* **2005**, *109*, 20433−20443. (b) Quartarolo, A. D.; Russo, N.; Sicilia, E. *Chem.—Eur. J.* **2006**, *12*, 6797−6803.

(23) Burghart, A.; Kim, H.; Welch, M. B.; Thoresen, L. H.; Reibenspies, J.; Burgess, K. *J. Org. Chem.* **1999**, *64*, 7813−7819.

(24) (a) Wang, W.; Rusin, O.; Xu, X.; Kim, K. K.; Escobedo, J. O.; Fakayode, S. O.; Fletcher, K. A.; Lowry, M.; Schowalter, C. M.; Lawrence, C. M.; Fronczek, F. R.; Warner, I. M.; Strongin, R. M. *J. Am. Chem. Soc.* **2005**, *127*, 15949−15958. (b) Tang, B.; Xing, Y.; Li, P.; Zhang, N.; Yu, F.; Yang, G. *J. Am. Chem. Soc.* **2007**, *129*, 11666−11667. (c) Fujikawa, Y.; Urano, Y.; Komatsu, T.; Hanaoka, K.; Kojima, H.; Terai, T.; Inoue, H.; Nagano, T. *J. Am. Chem. Soc.* **2008**, *130*, 14533−14543. (d) Hong, V.; Kislukhin, A. A.; Finn, M. G. *J. Am. Chem. Soc.* **2009**, *131*, 9986−9994. (e) Chen, X.; Zhou, Y.; Peng, X.; Yoon, J. *Chem. Soc. Rev.* **2010**, *39*, 2120−2135. (f) Lee, J. H.; Lim, C. S.; Tian, Y. S.; Han, J. H.; Cho, B. R. *J. Am. Chem. Soc.* **2010**, *132*, 1216−1217.

(25) Zhao, C.; Zhou, Y.; Lin, Q.; Zhu, L.; Feng, P.; Zhang, Y.; Cao, J. *J. Phys. Chem. B.* **2011**, *115*, 642−647.

(26) (a) Wright, A. T.; Anslyn, E. V. *Chem. Soc. Rev.* **2006**, *35*, 355−360. (b) James, T. D. *Top. Curr. Chem.* **2007**, *277*, 107−152. (c) Kim, S. K.; Lee, D. H.; Hong, J. I.; Yoon, J. *Acc. Chem. Res.* **2009**, *42*, 23−31.

(27) (a) Lee, M. H.; Kim, H. J.; Yoon, S.; Park, N.; Kim, J. S. *Org. Lett.* **2008**, *10*, 213−216. (b) Kim, H. J.; Park, S. Y.; Yoon, S.; Kim, J. S. *Tetrahedron.* **2008**, *64*, 1294−1300. (c) Kowalczyk, T.; Lin, Z.; Voorhis, T. V. *J. Phys. Chem. A* **2010**, *114*, 10427−10434.

(28) Tahtaoui, C.; Thomas, C.; Rohmer, F.; Klotz, P.; Duportail, G.; Mély, Y.; Bonnet, D.; Hibert, M. *J. Org. Chem.* **2007**, *72*, 269−272.

(29) Lin, W.; Long, L.; Tan, W. *Chem. Commun.* **2010**, *46*, 1503−1505.

(30) Frisch, M. J. et al. *Gaussian 09, Revision D.01*; Gaussian, Inc.: Wallingford, CT, 2009.